



Contents lists available at ScienceDirect

Gondwana Research

journal homepage: www.elsevier.com/locate/gr

Trends in physical, optical and chemical columnar aerosol characteristics and radiative effects over South and East Asia: Satellite and ground-based observations

S. Ramachandran^{a,b,*}, Maheswar Rupakheti^b^a Physical Research Laboratory, Ahmedabad, India^b Institute for Advanced Sustainability Studies, Potsdam, Germany

ARTICLE INFO

Article history:

Received 6 July 2021

Revised 6 September 2021

Accepted 11 September 2021

Available online xxxxx

Handling Editor: M. Santosh

Keywords:

Atmospheric aerosols

Physical

Optical and chemical characteristics

Radiative effects

Climate change

Asia

Aerosol trends

ABSTRACT

Recent satellite observations of atmospheric aerosol loading over Asia indicate a dipole pattern in the aerosol optical depth (AOD) with a substantial decrease in AOD over East Asia and persistent increase in AOD over South Asia, the two global hotspots of aerosol emissions. Aerosol emissions over Asia are also changing rapidly. However, the evolution of physical, optical and chemical columnar aerosol characteristics, and their radiative effects over time, and the resultant impacts of such evolving trends on climate and other associated risks are not yet properly quantified, and used in climate impact assessments. In order to do so, we closely examine, in addition to satellite observations, for the first time, high-quality, ca. two-decade long ground-based observations since 2001 of aerosols and their radiative effects from several locations in the Indo-Gangetic Plain (IGP) in South Asia and the North China Plain (NCP) in East Asia. A clear divergence in the trends in AODs is evident between the IGP and the NCP. The single scattering albedo (SSA) is increasing, and the absorption AOD due to carbonaceous aerosols (AAOD_{CA}) is decreasing over both regions, confirming that aerosols are becoming more scattering in nature. The trends in observed aerosol content (AOD) and composition (SSA) are statistically significant over Kanpur in the IGP and Beijing in the NCP, two locations with longest ground-based records. The aerosol radiative forcing of atmosphere (ARF_{ATM}) and resultant atmospheric heating rate (HR) are decreasing over both regions. However, current regionally coherent and high annual HR of 0.5–1.0 K day⁻¹ has severe implications to climate, hydrological cycle, and cryosphere over Asia and beyond. These results based on high-quality observations over a large spatial domain are of great significance and are crucial for modelling and quantifying aerosol-climate interactions.

© 2021 The Author(s). Published by Elsevier B.V. on behalf of International Association for Gondwana Research. This is an open access article under the CC BY-NC-ND license (<http://creativecommons.org/licenses/by-nc-nd/4.0/>).

1. Introduction

Atmospheric aerosols are either emitted directly into the atmosphere as particulate matter (primary aerosols) from natural and anthropogenic sources or formed in the air from gaseous precursors (secondary aerosols). Mineral dust, sea salt, black carbon (BC), organic aerosols (OA) and biological particles are primary aerosol particles, while sulfate, nitrate, ammonium and secondary OA (SOA) are mostly formed in the atmosphere from gaseous precursors. In the present-day scenario, mineral dust, sea salt and biological aerosols are predominantly of natural origin, while BC, organic carbon (OC), sulfate and nitrate emanate from anthro-

pogenic sources. The emissions of aerosols and their precursors exhibit large regional and seasonal variations (Samset et al., 2019). The characteristics of aerosol species such as the size, composition, and atmospheric lifetime vary widely across space and time (Myhre, 2013; Samset et al., 2019). In terms of aerosol mass, mineral dust contributes ~35% over urban South Asia and China, while sulfate and OC account for about 20% each, followed by nitrate, ammonium and BC (~5% each) (Myhre, 2013). Over the marine regions, sea salt is the dominant species and contributes ~60% to total aerosol mass (Myhre, 2013). Emissions of aerosols over Asia, mainly from anthropogenic activities, have been changing rapidly recently (Myhre et al., 2017; Samset et al., 2019). Satellite observations show that the aerosol content, expressed as aerosol optical depth (AOD), has been changing over Asia (Samset et al., 2019). Two countries, India and China, where ca. a third of the global population lives, emit ~40% of global BC and

* Corresponding author at: Physical Research Laboratory, Ahmedabad, India.
E-mail address: ram@prl.res.in (S. Ramachandran).

<https://doi.org/10.1016/j.gr.2021.09.016>

1751-7311/© 2021 The Author(s). Published by Elsevier B.V. on behalf of International Association for Gondwana Research.
This is an open access article under the CC BY-NC-ND license (<http://creativecommons.org/licenses/by-nc-nd/4.0/>).

primary OC aerosols (Myhre, 2017; IPCC, 2013). The large volume of aerosol emissions from developing countries, especially from Asia, contributes to increasing long-range transport of these emissions (Meng et al., 2019). Model simulations and satellite observations of aerosol emissions have shown that their geographical distributions have changed considerably over the last decade as a result of growing economic activities in various regions and introductions of air pollution control regulations in Asian countries with a primary emphasis on reducing adverse impacts of air pollution on public health, notably in China (IEA, 2016; Meng et al., 2019). In Asia, this has resulted in an emerging dipole (or divergence) in aerosol emissions between South Asia and East Asia (Samset et al., 2019) with a substantial decrease in emissions and atmospheric loadings over China accompanied with a coincidental persistent increase over India (Fig. 1a–c).

The uncertainty in the estimates of aerosol radiative forcing on climate globally is at least a factor of three (IPCC, 2013). The uncertainty associated with estimating the BC-induced atmospheric solar heating is one of the main agents contributing to this uncertainty. The aerosol absorptivity and aerosol-induced absorption are largely underestimated in many regions, in particular over Asia by current atmospheric models (IPCC, 2013; Myhre, 2013). East Asia and South Asia are global air pollution hotspots. The North China Plain (NCP) in East Asia and the Indo-Gangetic Plain (IGP) in South Asia are two most polluted regions in the world (Rupakheti et al., 2019; Ramachandran et al., 2020a,b). Quantitative analyses of long-term variations in aerosol content and composition from these aerosol hotspot regions are crucial for evaluating and predicting the climate effects of aerosols. Past studies on aerosol emissions and properties over Asia in general, and the IGP and the NCP in particular were based on (i) observational data at single or few locations, or for a limited observation time period or only few aerosol parameters (Kedia et al., 2014; Cho et al., 2017; Jethva et al., 2018; Rupakheti et al., 2019), (ii) inventories of aerosol emissions (Zheng et al., 2018), (iii) SO₂ emissions between 2005 and 2015 (Li et al., 2017), and (iv) multi-model simulations of radiative forcing estimates (Myhre et al., 2017). Using AOD time series obtained from the Along-Track Scanning Radiometers (ATSR: ATSR-2 and Advanced ATSR (AATSR)) AATSR Dual View (ADV), and MODIS data (version 6.1) AOD tendency estimations were reported (Sogacheva et al., 2018). Analysis showed that the AOD tendency over China exhibits seasonal and regional variations. The AOD was found to gradually decrease after 2011 with an average reduction in the range of 20–50% between 2011 and 2017, and the decreasing effect was more visible in the highly populated and industrialized regions in Southeast China (Sogacheva et al., 2018). (Jethva et al., 2019) reported trends in AODs using observations with the Aqua MODIS Multi-Angle Implementation of Atmospheric Correction (MAIAC), over the IGP for 2002–2016 period. An increase in AOD of 0.0187 per year during the post-monsoon and 0.0168 per year during the winter over the IGP was reported; this increase was attributed to a positive (increasing) trend in agricultural fires as a major factor in addition to the increase in fossil fuel burning emissions during the same period ((Jethva et al., 2019)). Che et al. (2019) examined the spatial distribution of aerosol microphysical and optical properties, and aerosol direct radiative forcing using the data collected with the China Aerosol Remote Sensing Network. The annual mean effective radius of aerosols was found to decrease from north to south and from rural to urban sites, and over the urban sites the particle volume concentrations were found to be higher. The AOD over China showed significant variation between remote and rural sites (0.12), and urban locations (~0.80) (Che et al., 2019). The climatology of AOD and radiative effects over Southeast Asia using 18-years of AERONET data were investigated using level 1.5 AERONET data (Khan et al., 2019). It must be noted that the level 1.5 AERONET data is cloud-screened

but without final calibration being applied, and thus, are not quality assured.

A few previous studies (Menon et al., 2002; Ramanathan et al., 2007a) have reported aerosol impacts on climate, the impacts on hydrological cycle and monsoon in Asia using model-simulated aerosol characteristics and trends. However, it may be noted that aerosol absorption in many regions is grossly underestimated by the models (IPCC, 2013; Shindell, 2013); Ramachandran et al., 2015; Ramachandran et al., 2020a,b). Therefore, model simulated aerosol characteristics and the trends in aerosol impacts such as on the climate, climate change, changes in precipitation and hydrological cycle over these regions may not be exactly representative because there are significant uncertainties and limitations in satellite data, representation of aerosols in models, and lack of observation-based analysis of trends in aerosol properties and their radiative effects. As the changing distribution patterns of aerosols in Asia is likely changing the extent of the aerosol radiative forcing in the region and beyond (Fig. 1), which is expected to be different from those observed in the late twentieth century with the different aerosol regime (Samset et al., 2019), it is crucial and need of the hour to have a complete, comprehensive and a more accurate analysis of aerosol characteristics over this region. The rapidly evolving aerosol characteristics over East Asia and South Asia may trigger large scale atmospheric responses which will have wide-ranging impacts on atmospheric processes, chemistry, clouds, climate, cryosphere and hydrological cycle, extending well beyond source regions in Asia (Hoegh-Guldberg et al., 2018; Samset et al., 2019).

We use satellite aerosol data - AOD, SSA (single scattering albedo, which is the ratio of scattering AOD to total AOD (scattering AOD + absorption AOD), aerosol absorption measured in terms of absorption AOD (AAOD) - to elucidate the temporal change in aerosols, as it has the advantage in terms of wider spatial coverage. The analysis of satellite retrieved parameters is constrained as the errors and uncertainties in satellite retrievals are higher than that of the in-situ measurements, and the retrieved aerosol parameters are a few, namely, AOD, SSA and AAOD as compared to the in-situ measurements, and have limited temporal resolution (e.g., Ramachandran et al., 2015) (further details are given in Results and Discussion). Further, apart from the changes and trends in AOD, SSA and AAOD, trends in other key climate-relevant aerosol parameters, such as aerosol radiative forcing (ARF), aerosol radiative forcing efficiency (ARFE), and aerosol-induced atmospheric heating rate (HR), have not been reported over Asia. They are fundamental to understanding the complex aerosol-clouds-climate interactions. Furthermore, the three major light-absorbing aerosols, i.e., dust, BC and brown carbon (BrC, i.e., light-absorbing OC) co-exist in significant amounts over Asia. The changes in dust, BC and BrC, including their trends and proportional contributions to AAOD in Asia over the last 2-decades have not yet been properly quantified. This knowledge is crucial to constrain the uncertainty in aerosol absorption. Given its large size, extremely varying physiological setting, a variety of land-ocean-atmospheric processes that vary across spatial and temporal scales govern the climate over Asia. It is therefore a challenging task to properly represent, simulate and predict or project the implications of such emerging patterns of aerosol loadings and their radiative forcings on climate and other regional processes and ecosystems (Samset et al., 2019).

In this study, we conduct a first-of-its-kind comprehensive investigation, and analyze the trends in columnar aerosol content, composition, absorption due to three major light-absorbing species (mineral dust, BC and BrC), ARF, ARFE and HR, and then discuss the climate implications of the findings using nearly 2-decade long high-quality ground-based columnar aerosol observations over several locations and satellite measurements covering a large spatial domain spanning from northern South Asia to East Asia, the

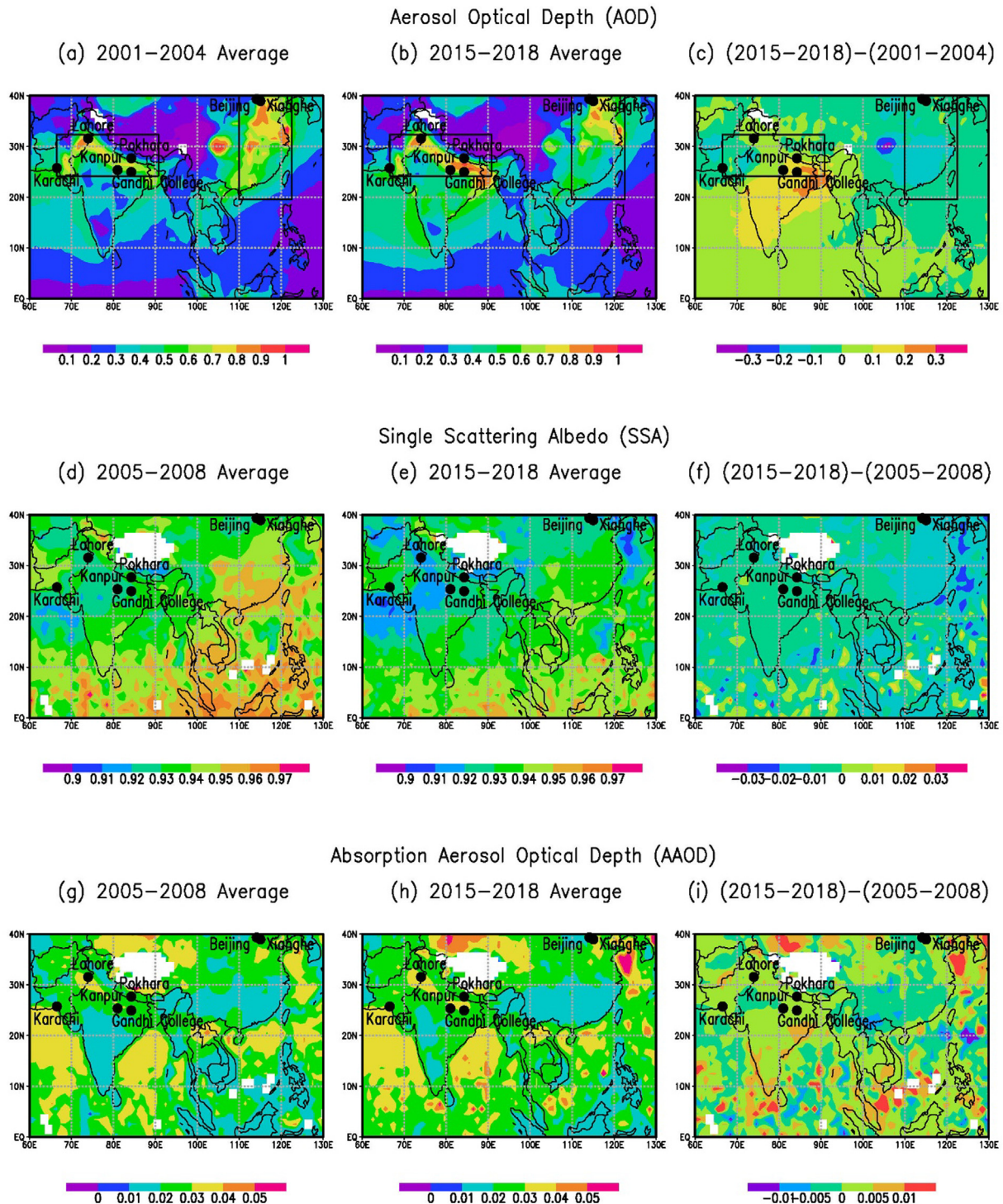


Fig. 1. Satellite observations of changing aerosol patterns over Asia. MODIS Terra version 6.1 daily AOD (a) average for 2001–2004 and (b) average for 2015–2018, and (c) the difference between 2015–2018 average and 2001–2004 average. OMI OMAERUV v003 daily level-2 SSA (d) average for 2005–2008 and (e) the average for 2015–2018, and (f) the difference between (e) and (d). OMI OMAERUV v003 daily level-2 AAOD (g) average for 2005–2008, (h) average for 2015–2018 and (i) the spatial difference between 2015–2018 average and 2005–2008 average. The MODIS AOD data correspond to a wavelength of $0.55 \mu\text{m}$, and OMAERUV v003 SSA and AAOD data correspond to a wavelength of $0.388 \mu\text{m}$, respectively. The MODIS AOD data were downloaded from <https://giovanni.gsfc.nasa.gov/giovanni/>, and SSA level-2 data were downloaded from https://disc.gsfc.nasa.gov/datasets/OMAERO_003/summary. All the study locations in South and East Asia are marked in the figure.

region home to large population and several sensitive ecosystems of global importance.

To achieve the above objectives, we have analyzed a huge dataset of the data collected at 12 AERONET sites in South Asia and East Asia, combined with satellite observations, and used the most recent data as well covering the period of 2001–2018. In an earlier

study (Ramachandran et al., 2020a) we presented trends in only three parameters (AOD, SSA and HR) during 2001–2017 and only over two sites - Kanpur in South Asia and Beijing in East Asia and then provided conclusions on HR with some broader implications. In the present study, we have used trends in (1) AOD and (2) SSA obtained during 2001–2018 (using ground-based as well as

satellite observations) as background information to derive trends in other multiple aerosol parameters, which include (3) contribution of fine mode fraction (FMF) of aerosols to AOD, (4) Angstrom exponent (α), (5) AAOD, (6) absorption Angstrom exponent (AAE), (7) ratio of AAOD to AOD, individual contributions of carbonaceous aerosol (CA) and dust AAOD to AAOD, i.e., (8) AAOD_{CA} and (9) AAOD_{Dust}, and further quantifying the contributions of BC and BrC to AAOD_{CA}, i.e., (10) AAOD_{BC} and (11) AAOD_{BrC} (thereby providing a very unique, new and comprehensive regional analysis of absorbing aerosols), aerosol radiative forcing (ARF) (12) at the surface (ARF_{SFC}), (13) in the atmosphere (ARF_{ATM}) and (14) at the top of the atmosphere (ARF_{TOA}), aerosol radiative forcing efficiency (ARFE) (15) at the surface (ARFE_{SFC}), (16) in the atmosphere (ARFE_{ATM}) and (17) at the top of the atmosphere (ARFE_{TOA}), and (18) aerosol-induced atmospheric heating rate (HR). This present study is massively more comprehensive than previous studies including Ramachandran et al. (2020a), and provides the most complete quantitative analysis yet of the observed aerosol properties required to simulate and quantify better the aerosol-climate interaction over South and East Asia. The trends in all the above mentioned 18 aerosol parameters are analyzed and presented for five other sites too, besides Kanpur and Beijing, in the region (Karachi and Lahore in Pakistan, Gandhi College in India, Pokhara in Nepal, and Xiang He in China) covering a vast region in South Asia and East Asia.

Such a regional-scale analysis including the trends in all the aerosol physical, optical, chemical and radiative parameters, unavailable so far, are crucial for modeling and quantifying the climate impacts due to aerosols over Asia which is quite uncertain (Samset et al., 2019; Krishnan et al., 2019). Further, these results provide an important framework and backdrop due to decrease or increase in aerosol emissions that have occurred in a phased manner *vis-à-vis* a sudden, abrupt and a lockdown enforced as a result of pandemic due to Corona Virus Disease 2019 (COVID19) (e.g., Cao et al., 2021), and its impact on aerosol characteristics. For instance, the PM_{2.5} (particulate matter of diameter <2.5 μm) were found reduced by 40% over China and India during lockdown resulting in improved air quality (Cao et al., 2021). The concentrations of atmospheric aerosols decreased due to reduction in emissions as a result of closure of cities, restrictions on vehicular movement, shutdown of industries, factories and restaurants (Cao et al., 2021). It is very important here to note that to assess and estimate the radiative and climate impact of aerosols, a quantitative analysis of columnar physical, optical and chemical aerosol characteristics and their trends are the crucial inputs, which is the focus of the current study, whereas an analysis of improvement in air quality due to measures such as lockdown can offer insights on mitigation strategies and reduction in aerosol pollution.

2. Data and analysis

2.1. Satellite observations over Asia

Data products from two satellite platforms are utilized: (1) the MODIS Terra AOD data (version 6.1 Combined Dark Target and Deep Blue Land and Ocean daily AOD data at 0.55 μm), and the (2) the Ozone Monitoring Instrument (OMI) SSA and AAOD data (OMAERUV v003 level-2 SSA and AAOD data at 0.388 μm). The error in MODIS Terra version 6.1 daily AOD over land and ocean are $\pm(0.05 \pm 0.15\text{AOD})$ and $\pm(0.03 \pm 0.05\text{AOD})$, respectively (Levy et al., 2013). Year-round OMI OMAERUV v003 daily level-2 SSA and AAOD data became available starting from 2005. It should be noted here that since mid-2007 a possible external obstruction affected the OMI observations that perturbed both the measured solar flux and Earth radiance (Torres et al., 2018). The viewing

geometry is associated with the row numbers on the charge-coupled device detectors, and the obstruction that has affected the quality of radiance at all wavelengths for a particular viewing direction. It is therefore referred to as “row anomaly” (Torres et al., 2018). For more details on the row anomaly, the readers are directed to previous publications (Torres et al., 2018; Ramachandran et al., 2020a). In this study we have utilized OMI SSA (level-2 OMAERUV product) derived from using only the first 23 rows that are unaffected by the row anomaly throughout the OMI operation. Torres et al. (2018) reported that SSA derived using radiances measured from 1 to 30, and 31–60 rows agree over regions dominated by sulfate or carbonaceous particles. (Jethva et al., 2014) found a 69% matchups in global comparison of OMI-AERONET SSA data with the absolute difference within ± 0.05 for all aerosol types. The root-mean-square error for OMI AAOD is estimated to be ~ 0.01 (OMI DUG, 2012).

2.2. Measurements of aerosol parameters at AERONET sites

The columnar aerosol amount, composition, and aerosol radiative forcing measured at the AERONET (Holben et al., 2001) (<https://aeronet.gsfc.nasa.gov/>) sites in South Asia (Karachi and Lahore in Pakistan, Kanpur and Gandhi College in India, and Pokhara in Nepal) and East Asia (Beijing and Xianghe in China) (Table 1) are analyzed. Our analysis provides a previously unavailable picture of regional and temporal trends in aerosol pollution over South Asia and East Asia. The IGP, which spans from Pakistan to the west, through India and Nepal, and Bangladesh to the east, is a densely populated, industrialized and a heavily polluted region in South Asia (Ramathan et al., 2007a, b; Ramachandran et al., 2015). The IGP and downwind regions, including northern Indian Ocean, are covered with a blanket of haze, almost throughout the year, loaded heavily with a wide variety of different aerosol types (dust, BC, nitrate, sulfate and organics) emitted from natural and anthropogenic sources in South Asia (Ramanathan et al., 2007a,b). Beijing, located in the NCP, is the world’s most populous capital city, and heavily industrialized and highly polluted megacity (Zheng et al., 2018). Xianghe, located 45 km to the southeast of Beijing, is a rural area. Lahore is located in northwest IGP while Kanpur and Gandhi College are in central IGP. Kanpur is a city while Gandhi College is a rural area located at ~ 500 km downwind of Kanpur. Karachi is a coastal city with two seaports in the western IGP. It is the largest city in Pakistan, while Lahore is the second largest city in Pakistan located in the northwestern edge of IGP, ca. 1000 km up north from Karachi. Pokhara, a metropolitan city, is a valley in the central Himalayan foothills, ca. 50 km to the north from the northern edge of the central IGP.

The CIMEL Sun/sky radiometers at the NASA Aerosol Robotic Network (AERONET) sites measure the direct solar irradiance and diffuse sky irradiances in the 0.34–1.02 μm range of the spectrum which are used to derive AOD, FMF (fine mode fraction, i.e., fractional contribution of particles <1 μm radius to AOD), Angstrom exponent (α), SSA, AAOD, Absorption Angstrom exponent (AAE), ARF and ARFE (Holben et al., 2001). In this study, we have used quality-checked (the level 2, version 3, cloud-screened and quality-assured) daily data collected at the AERONET sites from 2001 to 2018. The details of the time-periods for each site are mentioned in Table 1. The level 2, version 3 algorithm of AERONET is updated with respect to the previous version and includes improved cloud screening and quality control methods, cirrus cloud detection and removal (Giles et al., 2019). It may be noted that the AERONET level 2 data is quality assured data with the final calibration (pre- and post-) applied, cloud screened and manually inspected as opposed to level 1.5 data which are not quality assured and may not have final calibration applied. In the present work, the quality-assured daily mean aerosol properties corre-

Table 1

Details of AERONET sites located in South Asia and East Asia the data of which are used in the study.

Location	Latitude (°N)	Longitude (°E)	Elevation (m) (ASL [*])	Environment	Data coverage
1. Kanpur, India	26.5	80.2	123	Urban	2001–2018
2. Gandhi College, India	25.9	84.1	60	Rural	2006–2018 ⁺
3. Beijing, China	39.9	116.4	92	Urban, Industrial	2002–2018 ⁺
4. Xianghe, China	39.8	116.9	36	Rural	2005–2016
5. Karachi, Pakistan	24.9	67.1	49	Urban, Coastal	2009–2017 ⁺
6. Lahore, Pakistan	31.5	74.3	209	Urban, Industrial	2020–2016
7. Pokhara, Nepal	28.2	83.9	800	Urban	2010–2017

^{*} ASL – above sea level. ⁺Data for 2001 and 2005 over Beijing, for 2008, 2010, 2011, 2013 and 2017 over Gandhi College, and for 2013 over Karachi are not included in the analysis (see text for details). Gandhi College is located in Mirdha, a village that is about 10 km from Ballia in Uttar Pradesh, India.

sponding to individual observations are used to calculate the annual means and utilized.

Kanpur (since 2001) and Beijing (since 2001) stand as the only two sites in the entire South Asia and East Asia, respectively, with the longest records of AERONET measurements. The main criteria for inclusion in the analysis is that the data should cover all the four seasons (winter: December–February, pre-monsoon: March–May, monsoon: June–September, and post-monsoon: October–November) in a year, and the data is available during the year for ≥ 9 months. Following this, in case any AERONET site considered in this study had incomplete data for a year that particular year has been excluded in the analysis (2001 and 2005 in case of Beijing (data available only for 3 months during March–May in 2001 and Oct–Dec during 2005), and 2008, 2010, 2011 and 2013 in case of Gandhi College where data was available only for 3 months or less in these years) (Table 1). We have considered in this study only those sites in South and East Asia where all the aerosol parameters including AOD, SSA and ARF are available on a continuous basis. Further, only level 2 AERONET AOD data are available from 2009 to 2017 over Jaipur (26.91°N, 75.81°E, 450 m) in the IGP (SSA and ARF are not available), and other AERONET locations in NCP – Taihu (31.42°N, 120.21°E, 20 m), Xinglong (40.39°N, 117.58°E, 899 m), and Hong Kong (22.30°N, 114.18°E, 30 m) the SSA and ARF data are not available on a continuous basis to facilitate a trend analysis. Other locations in NCP in China, such as Xuzhou (34.22°N, 117.14°E, 59 m) and Hefei (31.91°N, 117.16°E, 36 m), and a couple of other locations in South Asia such as Lumbini (27.5°N, 83.3°E, 110 m), Kathmandu (27.7°N, 85.4°E, 1297 m) in Nepal, and Dhaka (23.7°N, 90.4°E, 34 m) and Bhola (22.3°N, 90.8°E, 7 m) in Bangladesh in IGP do not have level 2 AERONET data for more than a year or two (<https://aeronet.gsfc.nasa.gov/>), restricting us to not include these locations in the trend analysis.

The uncertainties associated with various aerosol parameters in the AERONET measurements are discussed in earlier publications, and are briefly summarized here. The uncertainty in the AODs is ± 0.01 for wavelengths $> 0.44 \mu\text{m}$ and is ± 0.02 for shorter wavelengths (Holben et al., 2001). The uncertainty is ± 0.03 in SSA when the AOD at $0.44 \mu\text{m}$ is > 0.2 (Dubovik et al., 2000), ± 0.01 in the AAOD (Mallet et al., 2013), $\sim \pm 10\%$ in the FMF (O'Neill et al., 2003). The aerosol properties retrieved by the AERONET have the highest accuracy for the observations made between 50° and 80° solar zenith angles (García et al., 2008). We have used only those data that satisfy this condition. The AERONET-derived AOD and SSA used in this study correspond to $0.55 \mu\text{m}$. The AODs and AAODs measured in the $0.44\text{--}0.87 \mu\text{m}$ wavelength range are used to estimate AE (α) and AAE, respectively. AAE is a determinant of the wavelength dependent aerosol absorption, and thus is an indicator of aerosol composition (Russell et al., 2010). AAE value also indicates the dominance of a specific type of light-absorbing aerosols (AAE is ca. 1 for aerosols containing BC, 1.5 for biomass burning aerosols, and 2 for mineral dust) (Russell et al., 2010).

2.3. Attribution of AAOD to dust, BC and BrC

Mineral dust, BC and BrC are three main light-absorbing aerosols. BC and BrC are collectively called light-absorbing carbonaceous aerosols (CA). BC and BrC are emitted together from biomass burning activities (residential cooking and heating, forest fires, agricultural fires, industrial use of biomass fuel) and fossil fuel combustion (from industries, transport and other activities). The deserts and arid regions are main sources of dust. In terms of light-absorption per unit, BC is the strongest with a SSA of 0.19 followed by BrC (0.85) and dust (0.84). However, as noted earlier, BC is a much smaller contributor to aerosol mass (5–10 times less) than the combined mass of BrC and dust. The BC light absorption (as 1-SSA) is over 5 times stronger than both BrC and dust. The BrC light absorption depends strongly on wavelength (effective over $0.3\text{--}0.6 \mu\text{m}$, falls very sharply after $0.4 \mu\text{m}$, and makes $< 5\%$ contribution beyond $0.55 \mu\text{m}$) (Kirillova et al., 2016). The light absorption by BrC is significantly less than BC. In this study we first estimate the contribution of dust and CA to AAOD (i.e., AAOD_{CA} and $\text{AAOD}_{\text{Dust}}$) following Chung et al. (2012). Then, the contribution of BC and BrC to AAOD_{CA} (i.e., AAOD_{BC} and AAOD_{BrC}) are estimated following Chung et al. (2012). For both, we made use of the AAOD values at 0.44 , 0.675 and $0.87 \mu\text{m}$ wavelengths. The readers are directed to Ramachandran et al. (2020b) for more details on this technique. As suggested in Chung et al. (2012) we assumed the AAE value of 2.4 for dust (AAE_{Dust}) and 1.16 for CA (AAE_{CA}). The AAE_{Dust} and AAE_{CA} vary across the source regions (AAE_{Dust} : 2.2–2.6, and AAE_{CA} : 0.84 for North America, West Europe and East Asia, 0.97 for East Europe, and 1.16 for South Asia) (Chung et al., 2012). In this study, the AAE_{CA} value of 1.16 was used for Kanpur, Gandhi College, Karachi, Lahore and Pokhara (located in South Asia), while 0.84 was used for Beijing and Xianghe (in East Asia). Furthermore, AAE_{BC} value of 0.5 and AAE_{BrC} of 4.8 were assumed to estimate AAOD_{BC} and AAOD_{BrC} , respectively (Chung et al., 2012). The AAOD, AAOD_{CA} , $\text{AAOD}_{\text{Dust}}$, AAOD_{BC} and AAOD_{BrC} reported in this study correspond to the wavelength of $0.55 \mu\text{m}$. The variations in AAE_{CA} and AAE_{Dust} lead to a maximum uncertainty of 16% in the derived contributions of AAOD_{CA} and $\text{AAOD}_{\text{Dust}}$ to AAOD (Ramachandran et al., 2020b).

2.4. Aerosol radiative forcing and atmospheric heating rates

The aerosol radiative forcing (ARF) is a function of (i) aerosol properties (AOD, SSA, asymmetry parameter), (ii) geophysical properties of the site (e.g., surface albedo), and (iii) position of aerosols and clouds (for deriving the vertical profiles of ARF), and (iv) solar insolation. García et al. (2012) reported that the effect of surface albedo on ARF was critical for accurately estimating ARF when surface albedo was > 0.30 and less critical when surface albedo was < 0.30 . The ARF at the surface (ARF_{SFC}) derived from the AERONET operational data is found to be overestimated because

the AERONET algorithms do not take into account upward fluxes with and without aerosols (García et al., 2012). Therefore, this overestimation needs to be corrected by multiplying the AERONET-derived ARF_{SFC} with (1-spectral average of surface albedo of the site) (García et al., 2012). In this study, we have applied this technique to correct the AERONET derived ARF_{SFC} . AERONET retrieval provides spectral surface albedo for each almucantar (almucantar refers to a series of measurements taken at the elevation angle of the Sun for specified azimuth angles relative to the position of the Sun) (Dubovik et al., 2000) retrieval (inversion algorithm product) in a day at the wavelengths of 0.44, 0.675, 0.87 and 1.02 μm . The annual-mean spectral average surface albedo in this spectral region for all the locations in the current study is <0.30 (Kanpur 0.23 ± 0.02 ; Beijing 0.15 ± 0.02 ; Karachi 0.24 ± 0.01 ; Lahore 0.19 ± 0.02 ; Gandhi College 0.22 ± 0.02 ; Pokhara 0.15 ± 0.01 ; Xianghe 0.18 ± 0.02). The \pm value, which is a standard deviation from the mean, represents the intra-annual variability; the inter-annual variations in the annual-mean spectral surface albedo values were negligible (they varied within 2%) over these locations during the study period.

The AERONET ARF values are instantaneous, and correspond to the time of measurement which are used to calculate annual means and then used in the present study. The minimum (begin) and the maximum (top) altitudes for flux calculations in AERONET are the elevation of each study location in msl (given in Table 1) and 120 km, respectively. AERONET ARF values are retrieved for atmosphere with aerosols present in the column only under the cloud-free clear-sky conditions. The AERONET retrieval algorithm uses a spheroid mixture as a generalized aerosol model (representing spherical, non-spherical, and mixed aerosols) (Dubovik, 2006), thereby accounting for non-spherical dust particles as well. The radiation fluxes with aerosols then are modeled using a mixture of spheroids and the detailed phase function (García et al., 2008), though the influence of particle shape on ARF is negligibly small (Mishchenko et al., 1997). The AERONET flux simulation depends on the retrieved real (RRI), and imaginary part (IRI) of refractive index (RI) of aerosols. The spectral integration uses RRI and IRI which are interpolated or extrapolated from the values of RI retrieved at the AERONET wavelengths (Dubovik, 2006). The AERONET flux calculations account for absorption and multiple scattering effects of aerosols (Dubovik, 2006; García et al., 2008). The GAME (Global Atmospheric Model) model, a radiative transfer model is used to perform radiative transfer calculations for gaseous absorption (Dubuisson et al., 1996) in which spectral integration is performed using correlated-k distribution based on line-by-line simulations. The instantaneous water vapor content retrieved by AERONET is used in the retrieval and ozone content is obtained from the NASA TOMS ozone climatology (García et al., 2008). The GAME model accounts for spectral gaseous absorption, for example, ozone in the UV-visible wavelength range, and water vapor in the shortwave IR spectrum (García et al., 2008). The atmosphere is assumed to be plane-parallel in AERONET retrievals where the vertical distribution of aerosols is assumed to be homogeneous in the almucantar inversion, and bi-layered for the principal plane inversion (Dubovik, 2006). The US standard 1976 atmosphere model is scaled to match the atmospheric gaseous concentrations in the column and used. The uncertainty in the AERONET calibrated sky radiance measurements is small, $\sim 5\%$ (Dubovik et al., 2000).

The AERONET retrievals are adequately sensitive to detect important minor features in spectral dependencies of RRI and IRI of the aerosol RI and in the spectral dependence of SSA (Dubovik et al., 2000; Andrews et al., 2017). An intercomparison of SSA from AERONET and in situ aircraft profiles during the DRAGON-MD and DISCOVER-AQ experiments found that all the coincident measurement pairs were within the accuracies of the measurement tech-

niques and the values were in excellent agreement (Schafer et al., 2014). It was also indicated that it was not possible to assess whether the in-situ measurements were biased low or the AERONET retrievals were biased towards high absorption (Andrews et al., 2017).

Aerosols can exist in different mixing states: external mixtures (when the different aerosol species such as sulfate, nitrate, organics, dust, BC, BrC, and sea salt, can co-exist without any physical or chemical interactions among themselves), core-shell mixtures (one aerosol species coats the other, i.e., BC particles coat sulfate aerosols or vice versa), and internal mixtures (all aerosol species get mixed together which results in a single aerosol entity). Different types of aerosol mixing states have been observed in several in situ field observations and were found to strongly vary with location and season (e.g., Zhang et al., 2003; Arimoto et al., 2006; IPCC, 2013). Due to different mixing states of aerosols their size distribution, life cycle and radiative effects can vary. In AERONET retrievals the SSA and ARF are retrieved for columnar aerosols using direct and diffuse radiances, and therefore the information on aerosol mixing is already embedded or accounted for while retrieving SSA and ARF. Further, it was found that for both cases of internally and externally mixed particles, no significant errors were observed in the AERONET retrieval of SSA (Dubovik et al., 2000).

García et al. (2008) reported an excellent agreement between the AERONET measured solar fluxes and the ground-based measurements with a correlation higher than 99% in all situations (mineral dust, maritime aerosols, biomass burning, urban-industrial, background continental, and free tropospheric aerosols). Previous studies (Ramachandran et al., 2012; Adesina et al., 2014) also found a very good correlation (correlation coefficient ≥ 0.90) between radiative forcing estimated by the model (using AERONET AOD, SSA and asymmetry parameter) and the AERONET radiative forcing at the top of the atmosphere (TOA) and at the Earth's surface (SFC) over two sites located in the IGP (Kanpur, an urban site and Gandhi College, a rural site), and over Pretoria (an urban site) in South Africa. To quantify the climate impact of aerosols the net gain/loss of energy at the surface, at the top of the atmosphere, and the net energy trapped in the atmosphere (ATM) are more crucial than their respective variations as a function of altitude. Earlier results have shown clearly that the inclusion of aerosol vertical profiles did not significantly alter the net ARF at TOA, SFC, and ATM and the aerosol-induced atmospheric heating rate (AHR) (Ramachandran et al., 2012; IPCC, 2013), because the net energy content trapped in the atmosphere was found to be the same in both the cases (with and without inclusion of aerosol vertical profiles). The degree to which the vertical profile of the aerosol distribution impacts ARF depends on many factors - the presence of clouds, SSA and surface albedo; and when absorbing aerosols (with an SSA of 0.7–0.8) are present above or below clouds they may affect ARF_{TOA} (e.g., (Choi, and Chung, 2014)). However, in the present study, the ARFs retrieved for the clear-sky atmosphere available from AERONET at SFC and TOA are used. The ARF in the ATM (ARF_{ATM}) is the difference between the ARF_{SFC} and ARF_{TOA} . Since the objective of the study is to determine the net energy trapped in the atmosphere (expressed in terms of atmospheric heating rate (HR)), non-inclusion of aerosol vertical profiles is not expected to modify any inferences or key results. The HR (in Kelvin day $^{-1}$) is estimated using the ARF_{ATM} and ΔP , which is the difference in atmospheric pressure between the elevation of each study location (given in Table 1) and 5,000 m asl over the site since most of the aerosols in the troposphere reside between the surface and 5000 m asl. This is a commonly used procedure for estimating the HR (Ramanathan et al., 2007a; IPCC, 2013).

2.5. Trend analysis

We used the linear regression method to calculate the trends in physical, optical, chemical and radiative properties of aerosols. It is a widely used method to estimate the trends in the time-dependent geographical variables. The linear regression method is a simple and robust method. It is also less sensitive to gaps in the time series of data. It is quite appropriate when the uncertainty in data is constant (i.e., Gaussian white noise) so that regression can be obtained by allocating a weight of unity (i.e., assigning the same precision) to each parameter (Ramachandran et al., 2012). It should be noted here that every site (Table 1) does not have AERONET level 2, version 3 data for the whole period of 2001–2018. For example, Karachi, Gandhi College and Pokhara have data only for eight years, and Lahore has data for only seven years during 2001–2018. The result of trend analysis on limited data is used only for providing general information on pattern in change (tendency) rather than a confirmation of trends. The statistical significance of the trends estimated is tested for a p -value <0.05 (at 95% confidence level).

3. Results and discussion

3.1. Satellite observations of AOD, SSA and AAOD

Satellite observations of aerosols over Asia clearly show a regional-scale dipole between East Asia and South Asia. They also show the decadal-scale changes in aerosol content (indicated by AOD) as well as composition (indicated by SSA and AAOD) within these regions (Fig. 1). Trends in satellite-derived AOD for the two sub-regions (i.e., IGP, NCP considered in this study) (Fig. 1) as well as over the two specific locations of Kanpur and Beijing located in the IGP and NCP, respectively (Fig. 2) for the observation period 2001–2018 are robust and similar, i.e., the AOD increases over a large polluted area in northern South Asia (boxed area) and Kanpur, and decreases over a similarly large area in East Asia (boxed area) and Beijing (Fig. 1). In the more recent years, the variation (i.e., as indicated by the standard deviation from mean shown in figures as vertical bars) in area-averaged AODs has been small (Fig. 2a, d), indicating a regional homogeneity in increase or decrease of aerosol emissions and hence atmospheric loading. Interestingly, trends show a notable contrasting feature between the two regions. The rate of increase is higher at local scale (Kanpur) in South Asia than the rate of increase in its wider surrounding region (Fig. 2a, g). On the other hand, over East Asia, the rate of decrease is twice as high over the broader surrounding region than that at the local scale of Beijing (Fig. 2d, j). However, though there are some differences in the magnitudes of rates of increase or decrease on larger region vs. local scale, there is an overall similarity in the trends in each region. Therefore, we show results of the two individual locations, Kanpur and Beijing, as being broadly representative of the respective regions in South Asia and East Asia, respectively. Both regions show negative (decreasing) trends in SSA (composition), however, the rate of decrease is slower than that of the AOD (Figs. 1 and 2).

AAODs remain more or less the same over the IGP, while they decrease over the NCP, during the observation period, however, the trends in AAODs are insignificantly small. The columnar AOD retrieved from satellites (e.g., MODIS) in general is more reliable than SSA and AAOD, as AOD represents the total column content of aerosols whereas SSA and AAOD depend on efficient and robust bifurcation of AOD into scattering and absorbing components. In addition, it should be noted that the performance of retrieval algorithms crucially depends on aerosol type, aerosol loading, and surface properties (Sayer et al., 2014). (Jethva et al., 2014) carried out

a comparative analysis of AERONET SSA and OMI SSA over 250 sites, and found that $<50\%$ of AERONET-OMI matchups agreed within the absolute difference of ± 0.03 . Although the root-mean square error in AAOD retrieved from OMI is comparable to AERONET AAOD, AAODs retrieved from OMI measurements are found to exhibit substantial biases (Shindell, 2013). The AAOD values are at least an order of magnitude smaller than AOD (Figs. 1 and 2). The retrieved AAOD values are close to the noise/errors, and exhibit large day-to-day variability resulting in a large standard deviation (Fig. 2). This is corroborated by the high p -values (i.e., less significant) in AAOD trends over regional (except NCP) as well as local scales (Fig. 2). The decreasing trends in SSA and AAOD are statistically significant over the NCP (p -value <0.001 at 95% confidence level). The agreement metrics between MODIS AODs and AERONET AODs are found to vary as a function of region and season (Sayer et al., 2014). Over the IGP, in particular where the aerosol loading is complex and consists of different aerosol types, the MODIS AODs are either underestimated or overestimated depending on the algorithm used (Dark Target or Deep Blue) (Sayer et al., 2014). The persistent underestimation of AODs in this region was attributed to an overestimated surface reflectance and/or overestimated aerosol SSA (Sayer et al., 2014). The discrepancies in data availability – daily average (mean) vs. monthly average can also lead to errors, for example, the monthly mean may not be the most appropriate summary metric and may not be an exact representative of monthly means, as daily averages are less sensitive to the manner in which averages are calculated (Sayer and Knobelspiesse, 2019); this is especially true for AOD distributions on monthly scales which are frequently closer to lognormal (Sayer and Knobelspiesse, 2019). Given the limitations with the data retrieved from satellites and their availability, in this study, we have used aerosol characteristics from the AERONET, which provides highly accurate measurements (Giles et al., 2019), and available almost continuously on a daily basis to derive the trends.

3.2. Ground-based AERONET observations

The results from in situ ground-based observations are arranged in the following manner – we begin with Kanpur in IGP, and Beijing in NCP, the two locations which have the longest records of level 2 version AERONET data in the last decades, followed by Karachi, Lahore, Gandhi College, Pokhara in IGP, and Xianghe in NCP.

3.2.1. Kanpur

Over almost 2-decades since 2001 the aerosol content (AOD), size (FMF, α), and composition (SSA, AAOD, AAE) changed over Kanpur (Fig. 3a–f). The annual mean AOD levels are in the 0.60–0.70 range, indicating that Kanpur was always highly polluted over the observation period of almost 2-decades. An increase in FMF and α suggest an increase in the abundance of fine aerosols during the last 2-decades. SSA, which was <0.90 in 2001 became >0.90 by 2018, indicating that the aerosol composition also changed making aerosols more scattering in nature, while the AAOD decreased, suggesting that the content and proportion of light-absorbing components of the aerosols decreased over this period.

AOD is directly proportional to aerosol loading, and the size distribution of aerosol mass burden in atmospheric column; typically, in the aerosol size distribution, number of fine mode aerosols are orders of magnitude higher than coarse mode particles. The aerosol size distribution plays a crucial role in determining the value of SSA as whether it is high or low depends on the ratio of the number of absorbing to scattering particles in a size distribution. AOD and SSA vary depending on the environmental setting, sources, meteorological conditions (relative humidity, winds, atmospheric boundary layer (ABL), rainfall, solar radiation) and dynamics (horizontal and vertical transport), and as a function of season. For example,

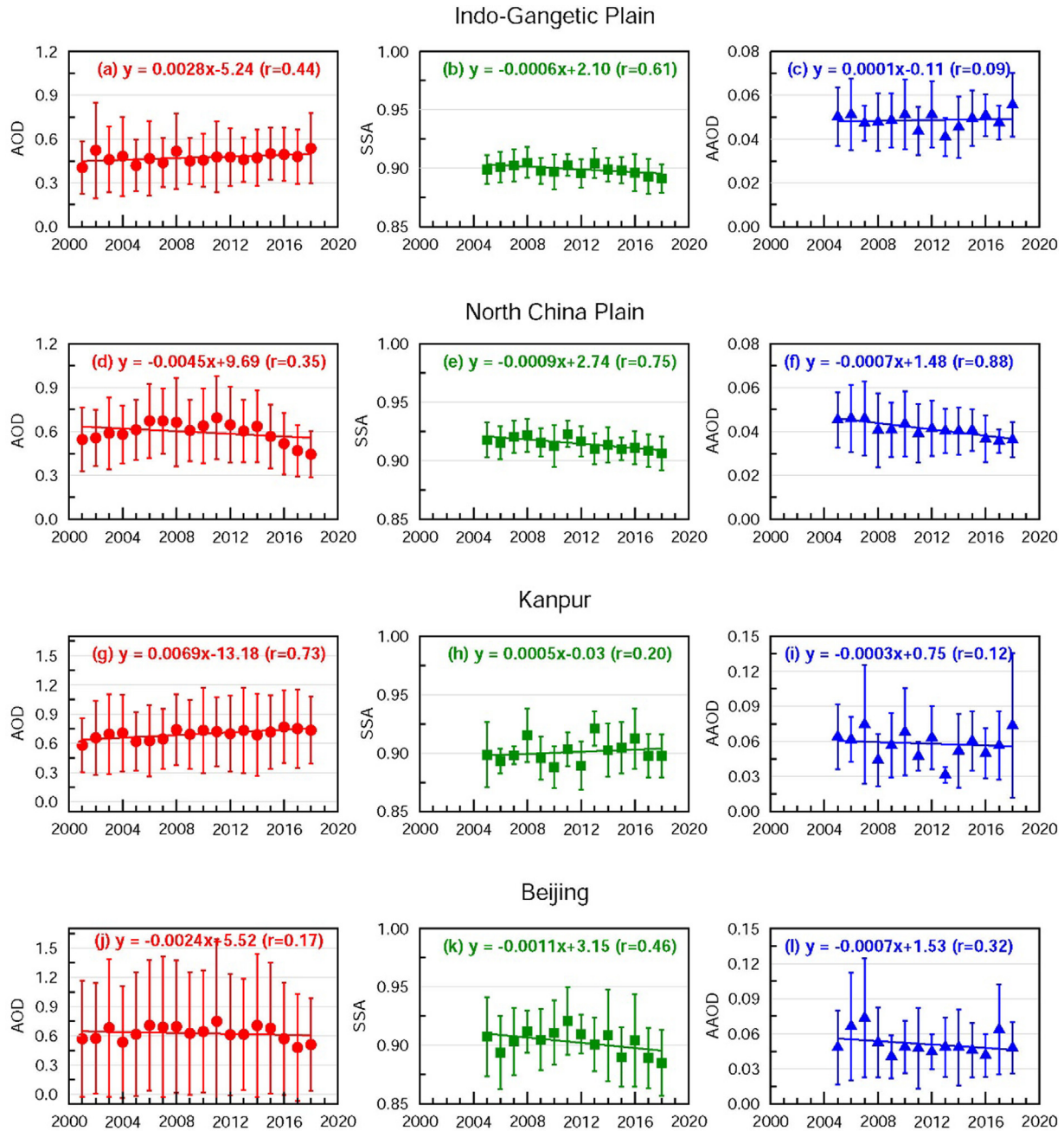


Fig. 2. Trends in satellite retrieved aerosol properties over the Indo-Gangetic Plain (IGP) in South Asia and the North China Plain (NCP) in East Asia: Area-averaged trends for IGP in (a) AOD (p-value 0.08, significance 0.06 at 95% confidence level (CL)), (b) SSA (p-value <0.001, significance 0.02) and (c) AAOD (p-value 0.83, significance 0.76), and for NCP in (d) AOD (p-value 0.13, significance 0.15), (e) SSA (p-value <0.001, significance 0.002) and (f) AAOD (p-value <0.001, significance <0.001 at 95% CL) (shown as boxes in Fig. 1). The trends for AOD, SSA and AAOD data over the grids where Kanpur and Beijing are located are shown in (g) AOD (p-value <0.001, significance <0.001 at 95% CL), (h) SSA (p-value 0.98, significance 0.49), (i) AAOD (p-value 0.65, significance 0.68) – Kanpur, and (j) AOD (p-value 0.44, significance 0.49), (k) SSA (p-value 0.03, significance 0.09) and (l) AAOD (p-value 0.25, significance 0.27 at 95% CL) – Beijing respectively.

weather conditions such as high wind speeds, low relative humidity, higher ABL heights, rainfall could favor an early dispersion of pollutants whereas unfavorable weather conditions (low wind speeds, higher relative humidity, lower ABL heights, less rainfall) may further worsen the air pollution scenario (e.g., Li et al., 2020). At a relative humidity of 80%, the AOD at $0.55 \mu\text{m}$ is about 0.06 for continental clean aerosols, an order of magnitude higher (0.64) for urban aerosols, ~ 0.30 for desert dust aerosols, and ~ 0.10 for maritime aerosols (Hess et al., 1998). In contrast to AOD, SSA is higher for continental clean aerosols (0.97) and decreases to ~ 0.82 for urban aerosols (Hess et al., 1998) whereas

the SSA for desert dust and maritime aerosols is 0.89 and 1.00, respectively. SSA is lower for an aerosol size distribution containing a higher amount of absorbing aerosols (e.g., BC in urban environment), while it is higher when scattering aerosols are dominant (e.g., sulfate, dust, maritime aerosols). The relation between SSA and AOD can be deemed to be contrasting or distinctive, because AOD is higher for urban aerosols whereas SSA is lower, and AOD is lower for continental clean, desert and maritime aerosols, however, their respective SSA are higher. However, it may be noted that such a distinguishable relation between AOD and SSA may not be evident in observations because the aerosols may have

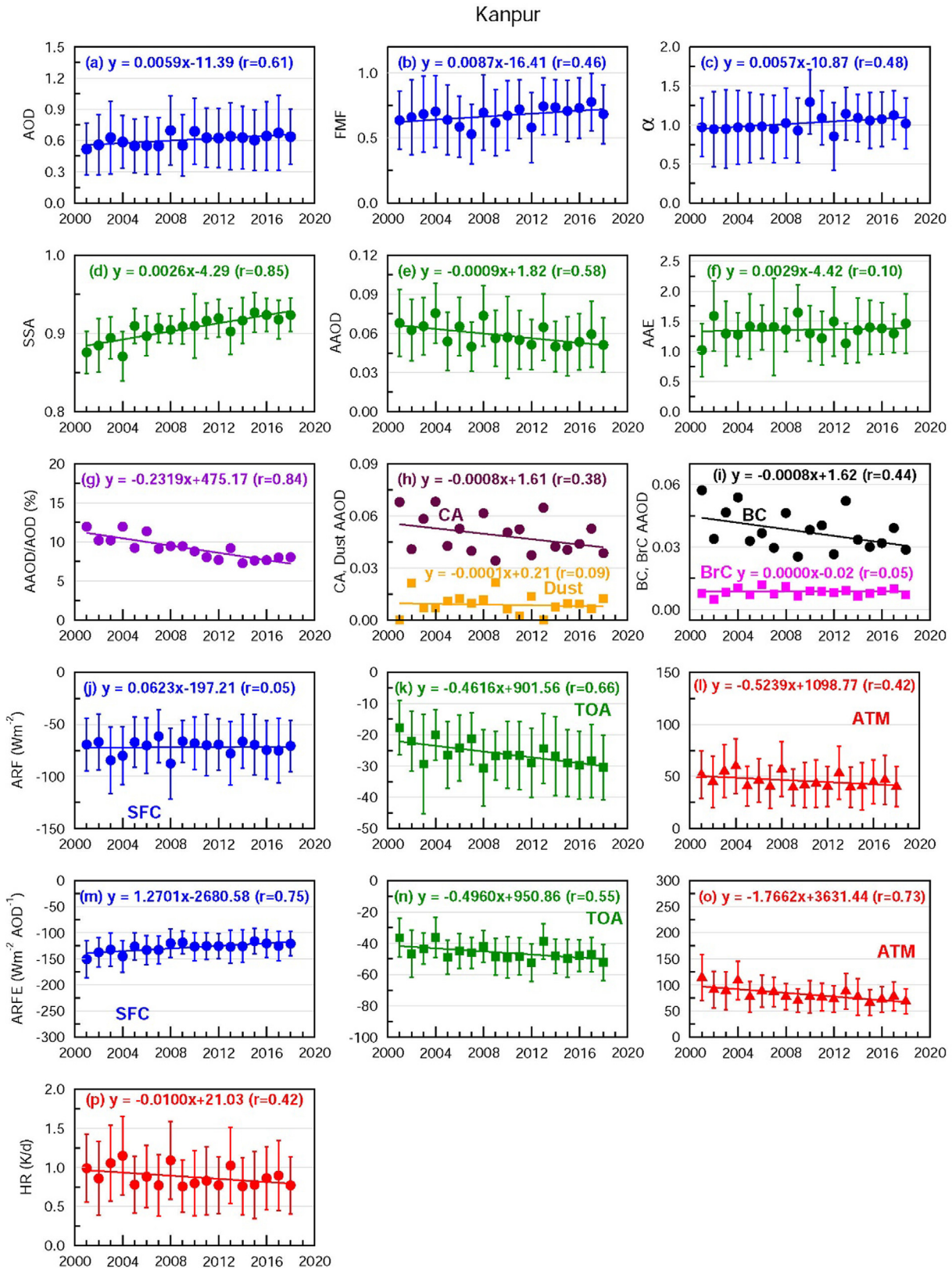


Fig. 3. Aerosol characteristics and radiative forcing over Kanpur in the Indo-Gangetic Plain (IGP), India based on the AERONET measurements during 2001–2018. Trends in (a) AOD, (b) FMF, (c) α , (d) SSA, (e) AAOD, (f) AAE, (g) AAOD/AOD (%), (h) AAOD_{CA} and AAOD_{Dust}, (i) AAOD_{BC} and AAOD_{BrC}, (j) ARF_{SFC}, (k) ARF_{TOA}, (l) ARF_{ATM}, (m) ARFE_{SFC}, (n) ARFE_{TOA}, (o) ARFE_{ATM} and (p) HR. Vertical bars indicate $\pm 1\sigma$ standard deviation from the annual mean.

additional components with varying number densities depending on the environment (Ramachandran and Rupakheti, 2020). Further, the relation between AOD and SSA is disparate is corroborated by

the fact that when the aerosol loading in the atmosphere decreases AOD also decreases, however, a reduction in AOD need not result in a change in SSA because SSA is determined by the ratio of scatter-

ing to absorbing aerosols. Therefore, for any change in SSA to occur the composition of aerosol distribution (ratio of scattering to absorbing aerosols) should change whereas for any change in AOD the aerosol loading comprising scattering and absorbing aerosols should change (increase or decrease). Thus, the corresponding relationship between the variation in the range of AODs and air quality is almost linear, i.e., air quality (visibility) improves as the atmospheric loading of particulate matter decreases and vice versa (Li et al., 2021; Cao et al., 2021). Air quality or visibility, a measure of level of air pollution is not only a primary public health concern but is equally important in the context of aerosol-climate interaction as the composition of particles present can influence the physical, optical and chemical properties of aerosols (e.g., AOD and SSA).

The AOD and SSA exhibit strong seasonal variability over the study region (IGP and NCP) (Ramachandran and Rupakheti, 2020; Cho et al., 2017; Che et al., 2019). AODs, in general, are higher during winter and post-monsoon seasons as compared to pre-monsoon and summer (monsoon) (Ramachandran and Rupakheti, 2020). A spatial gradient in AOD was evident from an urban, polluted location (high) to coastal, high-altitude location (low) over the study region. AOD over Karachi (0.3–0.6), a coastal city was lower than Kanpur (0.6–0.9), a city in central IGP during winter and post-monsoon, and > 0.3–0.6 during pre-monsoon and monsoon) (Ramachandran and Rupakheti, 2020). The annual average AODs were ≥ 0.3 at several sites over the IGP and the Himalayan foothills confirming that the study region is highly polluted. In contrast, the SSA was lower during winter (<0.95) due to dominance of light-absorbing carbonaceous aerosols and higher during monsoon (>0.95) due to wet removal of aerosols over the study region (Ramachandran and Rupakheti, 2020). Further, similar to AOD, a gradually decreasing west to east progression in SSA (high over Karachi to low over Pokhara) was found corroborating the presence of a gradient in the dominance of light-absorbing aerosols over the IGP (Ramachandran and Rupakheti, 2020). Likewise, SSA varied between 0.88 (urban) and 0.92 (rural, remote sites) in China indicating the dominance of strongly absorbing to slightly absorbing aerosols in China (Che et al., 2019). As mentioned earlier, in the observations the contrasting relation between AOD and SSA – AOD high, SSA low and vice versa is not clearly evident (e.g., Ramachandran and Rupakheti, 2020).

AAOD and SSA are anti-correlated, and hence their trends are of opposite signs. In absolute terms, the rate of decrease in AAOD is a factor of three lower than the rate of increase in SSA. The percentage contribution of AAOD to AOD decreased from $\sim 12\%$ in 2001 to $\sim 8\%$ in 2018. The annual average AAE over Kanpur is ≥ 1 during the 2-decades, suggesting the dominance of BC in aerosol absorption. The AAOD has a decreasing trend while AAE has a positive (increasing) trend, indicating the change in the content and composition of absorbing aerosols. Among the absorbing aerosols, the rate of decrease of dust contribution to AAOD is 8-times lower than that of AAOD_{CA}. Furthermore, among the carbonaceous aerosols, AAOD_{BC} decreased while AAOD_{Brc} does not show any trend during 2001–2018 (Fig. 3i). The AAOD_{BC} and AAOD_{CA} decreased at the same rate. BC's contribution to AAOD_{CA} over Kanpur was dominant ($\geq 75\%$ from BC and the rest from BrC (Fig. 3h, i)). It should be noted that both dust and BrC have very similar SSA values, and are at least 5-times less absorbing than BC. The increase in SSA values corroborated by the decreasing AAOD and AAOD_{BC} (which indicate decrease in the content of absorbing aerosols) clearly confirm that the aerosols have become more scattering in nature over Kanpur during the last 2-decades (Fig. 3d). The emissions from residential biomass fuel used for cooking and heating are the largest single sector influencing outdoor air pollution across most of India during 2015 (Venkataraman et al., 2018). Over India, the emissions of PM_{2.5}, BC and OC have been increasing, and were identical to the

increase in fuel consumption in the thermal power plants and industries (Sadavarte and Venkataraman, 2014). The increase in PM_{2.5} and SO₂ emissions from the industrial sector was ~ 2.5 times larger than the increase in fuel consumption, which was attributed to the growth in process emissions resulting from an increase in production activity. In the transport sector, the increase in above emissions was smaller than the corresponding increase in fuel consumption owing to implementation of emissions and fuel quality norms (Sadavarte and Venkataraman, 2014). The smaller increases in BC emissions from the transport sector, and the large regionally prevalent biomass burning (and its increase) result in decreasing AAOD_{BC} and an almost constant AAOD_{Brc} during the last 2-decades (Fig. 3i).

The ARF_{SFC} (Fig. 3j) shows a subtle but positive (increasing) trend while ARF_{TOA} (Fig. 3k) and ARF_{ATM} (Fig. 3l) have clear decreasing trends. ARF_{SFC} is influenced more strongly by the change in AOD than the change in SSA, while ARF_{TOA} is influenced more strongly by the change in SSA. ARF_{TOA} becomes more negative for higher SSA which is consistent with the observed increasing SSA values. The increasing ARF_{SFC} (Fig. 3i) during the 2-decades over Kanpur is consistent with the increasing trend in AOD (Fig. 3a). Both aerosol types - scattering and absorbing - cool the Earth's surface, while their radiative effects in the atmosphere vary with altitude. For the scattering aerosols (i.e., aerosols with higher SSA, e.g., sulfate), the ARF_{TOA} and ARF_{SFC} are quite similar in the shortwave region. In contrast, for the absorbing aerosols (aerosols with lower SSA, e.g., BC) the ARF_{SFC} is ~ 2 –3 times larger than the ARF_{TOA} in the shortwave region. Therefore, the absorbing aerosols lead to higher atmospheric warming. The relation between ARF_{SFC} and AODs is linear for aerosols with same SSA (i.e., the same type of aerosols). However, the ARF_{TOA} depends significantly on the SSA, and it can be either positive (for lower SSA) or negative (for higher SSA), unlike the greenhouse gas forcing which is always positive (Ramanathan et al., 2007a). The ARF_{ATM} (Fig. 3l), the difference between the ARF_{TOA} and ARF_{SFC}, shows a decreasing trend similar to ARF_{TOA} as it is also crucially dependent on the SSA. The ARFE, which is aerosol radiative forcing (Wm^{-2}) normalized to the AOD (Fig. 3m–o), serves as a very useful measure (as a further indicator beyond the SSA) to quantify the influence of absorbing and scattering properties of aerosols. The normalization rules out the influence of AOD on ARF and thus ARFE can be interpreted to be a measure of how much the atmosphere is forced radiatively per unit decrease or increase in AOD. The trends in the ARFE_{SFC}, ARFE_{TOA} and ARFE_{ATM} (Fig. 3m–o) are similar to the trends in corresponding ARF_{SFC}, ARF_{TOA} and ARF_{ATM} (Fig. 3j–l). The trends in ARFEs show that aerosols have become less efficient in modulating the radiation due to increase in AOD (SFC) and SSA (TOA, ATM) during the last 2-decades. The AHR is higher than 1 K day^{-1} over Kanpur during the last 2-decades (Fig. 3p) and shows a decreasing trend consistent with the decreasing trend in ARF_{ATM} (Fig. 3l). The trends in most aerosol parameters and radiative forcings are statistically significant for Kanpur with p-values lower than 0.01 at 95% confidence level (Table 2).

3.2.2. Beijing

Over almost 2-decades since 2002, the AOD over Beijing decreased substantially (Fig. 4a) while it increased over Kanpur (Fig. 3a), confirming a dipole in columnar aerosol loading between Kanpur and Beijing. The satellite observations show that such dipole also exists at the regional scale between East Asia and South Asia (Figs. 1 and 2). This will be further discussed in the subsection on aerosol trends at regional scale. The FMF and α show a decreasing trend over Beijing (Fig. 4b, c) in contrast to Kanpur, which confirms the presence of an aerosol dipole in the aerosol loading of fine and coarse mode particles. SSA shows an increasing trend (Fig. 4d), similar to Kanpur. The AAOD decreased by almost

Table 2

Details on the statistical tests for the trends in aerosol parameters and radiative effects over the AERONET sites located in South Asia and East Asia the data of which are used in the study. P-values are estimated at 95% confidence level. P-values ≤ 0.05 are highlighted in boldface.

Parameter	IGP					NCP	
	Karachi	Lahore	Kanpur	Gandhi College	Pokhara	Beijing	Xianghe
1. AOD	0.54	0.12	0.01	0.04	0.70	<0.01	0.14
2. FMF	0.64	0.04	0.05	0.30	0.36	0.03	0.73
3. α	0.84	0.14	0.07	0.73	0.92	0.13	0.88
4. SSA	0.14	0.04	<0.01	0.04	0.74	<0.01	0.41
5. AAOD	0.03	0.55	0.01	0.03	0.63	<0.01	0.65
6. AAE	0.06	0.69	0.75	0.71	0.34	0.03	0.17
7. AAOD/AOD (%)	0.06	0.28	<0.01	<0.01	0.46	0.77	0.46
8. AAOD _{CA}	0.03	0.92	0.11	<0.01	0.37	<0.01	0.18
9. AAOD _{Dust}	0.05	0.48	0.71	0.89	0.13	0.26	0.16
10. AAOD _{BC}	0.04	0.86	0.21	<0.01	0.53	<0.01	0.11
11. AAOD _{BrC}	0.01	0.37	0.66	0.62	0.07	0.01	0.83
12. ARF _{SFC}	0.33	0.38	0.76	0.52	0.99	<0.01	<0.01
13. ARF _{TOA}	0.01	0.13	<0.01	0.10	0.51	0.37	<0.01
14. ARF _{ATM}	0.06	0.62	0.07	0.88	0.89	<0.01	0.31
15. ARFE _{SFC}	0.02	0.07	<0.01	0.55	0.69	0.39	<0.01
16. ARFE _{TOA}	0.01	0.83	0.02	0.28	0.79	0.01	0.15
17. ARFE _{ATM}	0.01	0.06	<0.01	0.31	0.73	0.69	0.01
18. HR	0.06	0.62	0.07	0.88	0.89	<0.01	0.31

one-third (30%) during the 2-decades over Beijing (Fig. 4e). A significantly increasing trend concurrently in the AAE suggests a change in the amount of absorbing aerosol types contributing to aerosol absorption over Beijing (Fig. 4f). The ratio of AAOD to AOD remained almost same during the last two-decades (Fig. 4g), being about 10%, over Beijing which suggests that the contribution of aerosol absorption to AOD did not change significantly. However, the contribution of each absorbing aerosol type to absorption has been changing, which is evident in the trends in AAOD_{CA}, AAOD_{Dust}, AAOD_{BC}, and AAOD_{BrC} (Fig. 4h, i).

The rates of decrease in the AAOD_{CA} and AAOD_{BC} (Fig. 4h, i) are steep and more or less similar to each other, as was the case with them over Kanpur (South Asia) (Fig. 3h, i). However, the rates of decrease of AAOD_{CA} and AAOD_{BC} over Beijing are ~ 2.5 -times higher than that of Kanpur (Fig. 3). The AAOD_{Dust} shows a slight increasing trend over Beijing (in the absolute terms 6-times lower than AAOD_{CA}), while AAOD_{BrC} shows a very small decreasing trend over Beijing. Towards the end of the study period (i.e., 2018), the SSA decreases consistently with an increase in AAOD_{CA} and AAOD_{BC} (Fig. 4h, i). The SSA over Beijing (0.91) is 3.4% higher than over Kanpur (0.88) to begin with in 2002, and become almost the same towards the end of two decades (0.92–0.94) as a result of change in aerosol composition. The aerosol emissions, in particular anthropogenic emissions, over South Asia and East Asia have been changing since 2010 as a result of the introduction of more stringent air quality control measures widely aimed to address deteriorating air quality and the public health concerns. The emissions of sulfur dioxide (SO₂) (Li et al., 2017), and other pollutants including black carbon (BC) have been reduced more rapidly over China (Zheng et al., 2018) since 2010 due to the implementation of stringent air pollution control policies and climate policies while taking advantage of advances in the clean energy technologies. In China, in order to improve ambient air quality a series of laws and regulations were issued in the last decade, including the Air Pollution Prevention and Control Action Plan in 2013 and comprehensive three-year (2018–2020) action plan in 2018 (Li et al., 2020). Results showed that the Beijing's air quality improved noticeably over 2013–2019 (Li et al., 2020). The PM_{2.5} and SO₂ emissions decreased by $\sim 53\%$ and $\sim 85\%$ respectively in 2019 with respect their 2013 values (Li et al., 2020), which are consistent with the decrease in AOD over Beijing during this period (Fig. 3a, Ramachandran et al., 2020a). Beijing's air quality improved dominantly due to the significant reduction in coal-fired emissions (Li

et al., 2020). It is worth mentioning here that an exact one-on-one relation between PM_{2.5} and AOD, and between PM_{2.5} and SSA may be difficult to establish because of the fact that the PM_{2.5} measurements correspond to the surface level whereas AOD and SSA are columnar measures, and for the reasons discussed earlier on variations in aerosols on spatial, temporal and vertical scales, and aerosol types, the surface level air pollutant concentrations can be different when compared to the aerosol characteristics measured as a function of altitude as well as column (Ramachandran and Rupakheti, 2020).

Thus, an increase in SSA can be brought about by changing the proportions of the absorbing aerosols and the scattering aerosols. SSA can increase if either there is an increase in scattering aerosols (e.g., sulfate), and/or a decrease in absorbing aerosols (e.g., BC), as the SSA is controlled by the ratio of BC-to-sulfate in aerosol mixture (Ramana et al., 2010). Emissions of both SO₂ and BC have decreased over China recently (Li et al., 2017; Zheng et al., 2018). SO₂ emissions decreased by 62% over China during 2010–2017 while BC emissions decreased by 28% during the same period (Zheng et al., 2018). Significant difference in their rates of decrease can change the SSA. The decrease in BC emissions by 25% and the BC-to-sulfate ratio by 20% over Beijing modified the aerosol absorption (Ramana et al., 2010; Lim et al., 2018) which could have increased the SSA. (Lim et al., 2018) reported that, as sulfate increased gradually with increase in ambient relative humidity in a sulfate-dominated environment, absorption of BC and BrC got altered through the internal mixing of aerosols and the SSA of the aerosol mixture was enhanced. In addition, the relative contributions of biomass burning and fossil fuel combustion to BC emissions contrastingly differ between East and South Asia. The fossil fuel contribution to the total BC is 30–50% over South Asia, whereas it is about 60–80% over East Asia (Ramana et al., 2010; Ramachandran et al., 2020b). Furthermore, the change in proportion of the secondary organic aerosols (SOA), which are mostly scattering in nature, is also expected to alter SSA. SOA constitutes up to 70% of aerosol mass concentration in metropolitan areas, and is continuously increasing over China (Huang et al., 2014). Recently, it has been shown that particle size plays a key role in influencing the core-shell structure of organic matter (OM) and inorganic aerosols in addition to O/C ratios in ambient aerosols (Li et al., 2021). Further, it was found that internally-mixed OM coatings can have different effects on particle hygroscopicity when compared to externally-mixed OM. It was further emphasized that

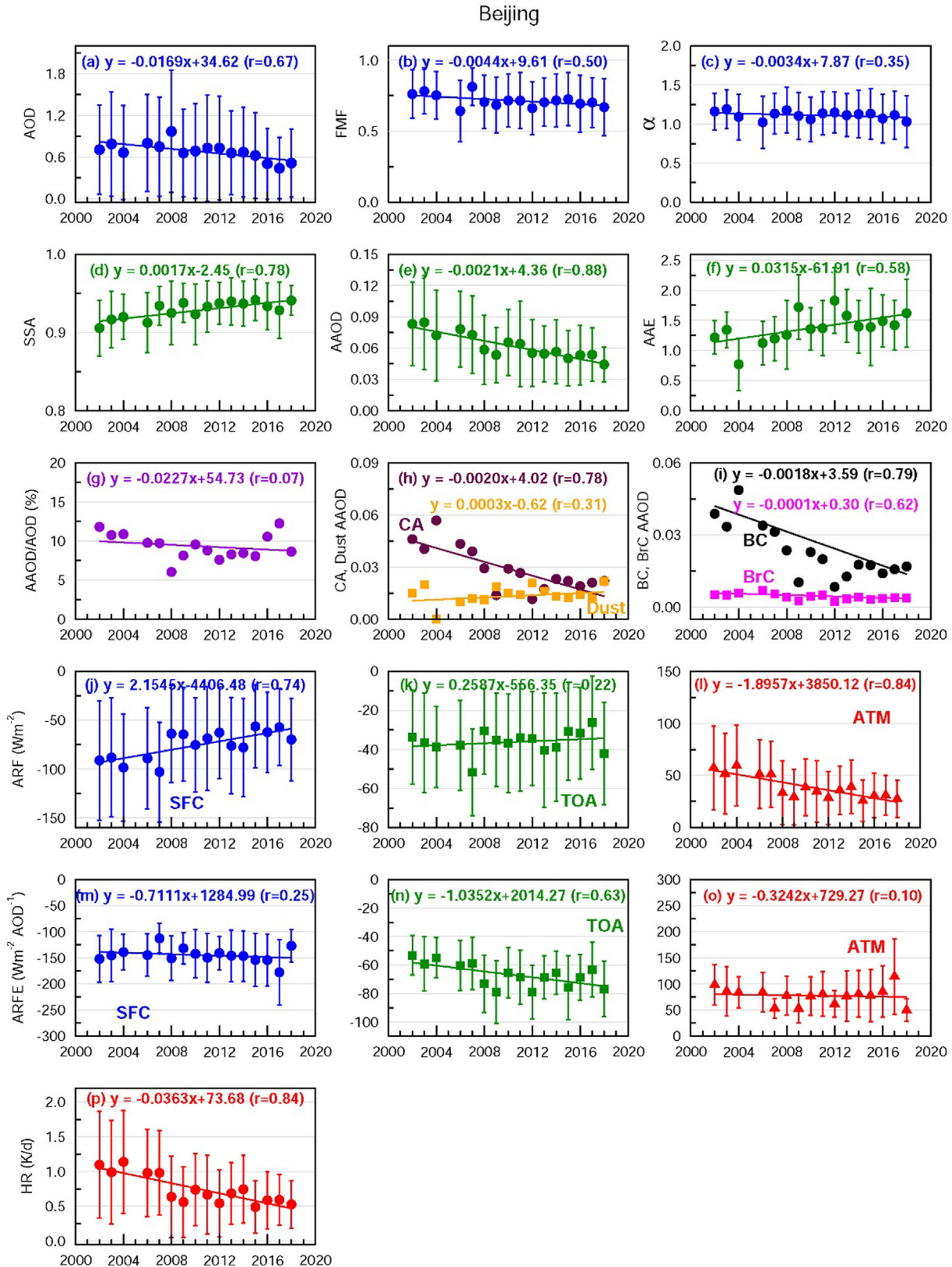


Fig. 4. Aerosol characteristics and radiative forcing over Beijing in the North China Plain (NCP), China based on the AERONET measurements during 2002–2018. The aerosol parameters are presented in the same order as in Fig. 3.

how phase separation phenomenon between organic and inorganic species in fine mode aerosol particles influences regional climate should be examined inasmuch as that a large fraction of SOA is

BrC in the NCP (Li et al., 2021) which has implications to variations in air quality, AOD and SSA. The decreases in SO_2 and BC emissions can also change the proportion of SOA, thereby increasing the SSA,

as seen earlier. The increase in SSA over Kanpur in South Asia (Fig. 3) is associated with the increasing SO₂ emissions in South Asia (Zheng et al., 2018).

The rate of increase in ARF_{SFC} (becomes less negative or in other words more solar radiation is reaching to the Earth's surface) over Beijing is significantly higher than the slightly increasing trend in ARF_{TOA}, though the absolute values of ARF_{TOA} is about a factor of 2 lower than ARF_{SFC} (Fig. 4j–l). The trend in ARF is a result of the balance between the strongly decreasing trend in AOD and an increasing trend in SSA. The ARF_{TOA} increases (becomes less negative) owing to SSA increase. The ARF_{ATM} over Beijing shows a strong decreasing trend, almost with a similar magnitude as that of the increasing trend in ARF_{SFC}. The AODs, ARF_{SFC} and ARF_{TOA} are higher over Beijing than over Kanpur (Fig. 4m–o). A higher ARF_E over Beijing suggests that the aerosols over Beijing are more efficient radiatively than Kanpur. The HR has decreased over both Kanpur and Beijing during the last 2-decades (Figs. 3 and 4). The magnitude of the heating rate is higher over Kanpur than Beijing because of lower SSA over Kanpur (Fig. 4p). The HR has remained consistently >0.8 K d⁻¹ every year during the 2-decades over Kanpur (Fig. 3p), while it decreased to ca. 0.5 K d⁻¹ over Beijing towards the end of the last decade. Also, it has decreased more rapidly over Beijing (~3-times faster) (Fig. 4p) than over Kanpur during 2001–2018, which is consistent with a 3-times faster decline in the AAOD due to the major absorbing aerosol component (BC) over Beijing. The trends in most of the aerosol parameters (AOD, FMF, SSA, AAOD, AAE, AAOD_{CA}, AAOD_{BC}, AAOD_{BrC}) and ARF (SFC, ATM), ARF_E (TOA) and HR are statistically significant for Beijing with p-values lower than 0.05 at 95% confidence level (Table 2).

3.2.3. Aerosol trends at regional scale

The trends in aerosol characteristics over Kanpur and Beijing are representative of the densely populated and heavily polluted centers in the Indo-Gangetic Plain (IGP) in South Asia and Northern China Plain (NCP) region in East Asia, respectively. Are these trends in aerosol properties and forcing regional in nature, and are they observed in the ground-based in situ observations at other locations in this region? Satellite observations (for example, observations in 2005 and after a decade in 2015) clearly show aerosol content (AOD) (also reported by Samset et al., 2019) as well as composition (SSA), and absorption (AAOD) have changed on regional-scale over Asia (Fig. 1). This feature is elaborately examined in this study by analyzing the aerosol characteristics over five other locations in South Asia (Karachi, Lahore, Gandhi College and Pokhara), and one more location in East Asia (Xianghe) which are located in environmentally different settings in these regions, and the results of which are discussed below. The time periods for which the AERONET data is available to perform the analysis is however shorter in these locations (Table 1) as compared to Kanpur and Beijing.

3.2.3.1. IGP (Karachi, Lahore, Gandhi College), and Himalayan foothills (Pokhara).

Generally, over all the five sites (including Kanpur) in South Asia the aerosol properties are regionally homogeneous, except for a few site-specific properties due to their proximity to uniquely different emission sources of aerosols. For example, most of them have witnessed increasing aerosol loading (positive trends in AOD, FMF, α), changing aerosol composition in such a way that they are becoming more scattering in nature (positive trends in SSA, and negative trends in AAOD, AAOD/AOD ratio, AAOD_{CA}, AAOD_{DUST}, AAOD_{BC}, AAOD_{BrC}), and hence resulting in a less aerosol-induced atmospheric heating (decreasing trends in ARF_E and HR). The trends in aerosol properties, both common to all sites and specific to individual site (Figs. 3 and 5–8), are discussed here.

The atmospheric loadings of aerosols (AODs) over four sites (Kanpur, Lahore, Gandhi College and Pokhara) in South Asia (Figs. 3 and 6–8) show a significant positive (increasing) trend while it shows a slight negative (decreasing) trend over Karachi (Fig. 5). FMF and α both show increasing trends over all the sites (including Kanpur). Over Karachi the annual mean FMF is always ≤ 0.5 , except 2015, indicating the major contribution of the coarse mode (>1 μm in radius) aerosols to AOD (Fig. 5b). The lower α value and its decrease are consistent with the smaller FMF and decreasing contribution of fine particles to AOD. Trends in aerosol properties over Gandhi College (Fig. 7) are similar to that of Kanpur indicating a regional homogeneity in variations in aerosols. AODs over Gandhi College are comparable to Kanpur (Fig. 3). FMF and α values are higher as compared to Kanpur which is consistent with lesser amount of coarse dust particles over Gandhi College (Kedia et al., 2014; Ramachandran et al., 2015; Ramachandran et al., 2020b). FMF over Pokhara (>75%), a site in the Himalayan foothills often downwind of the Indo-Gangetic Plain (Fig. 8), is higher than the other study locations in South Asia, indicating the dominance of fine mode aerosols in columnar aerosol loading, which is corroborated by the higher α values. The trends at all sites in this region indicate that the atmospheric aerosol loadings over this region have increased during the observation period.

In terms of change in aerosol composition, the SSA is comparatively lower over Gandhi College (Fig. 5d) than Kanpur (Fig. 3d) because Gandhi College is heavily influenced by local and regional biomass and biofuel burning emissions (which was evident in the significantly higher number of cloud-corrected fire counts (Kedia et al., 2014)), and transport of fossil fuel emissions from major urban centers (Ramachandran et al., 2015, 2020a). This is corroborated by the absorbing aerosol type, 'Mostly BC', which was always higher over Gandhi College than Kanpur. The annual mean (based on 5-years of AERONET data for 2006–2010) 'Mostly BC' absorbing aerosol type over Gandhi College (43%) was 11% higher than over Kanpur than Gandhi College (Kedia et al., 2014). SSA is relatively higher over Karachi, and AAOD is lower (Fig. 5). The AAE values are higher over Karachi indicating the dominance of dust in aerosol absorption, and the trend in AAE is increasing suggesting that the influence of dust over Karachi (Ramachandran et al., 2015, 2020b) is increasing which is also consistent with lower FMF and inter-annual variation (reflected in the standard deviation). Similarly, AAE shows an increasing trend over Pokhara. AAE shows increasing trends over Lahore and Gandhi College (Figs. 6f, 7f), and the values are >1.0 indicating that aerosol absorption is influenced by a mix of urban/industrial, and biomass burning emissions (Ramachandran et al., 2015).

The AAOD/AOD ratio, AAOD_{CA}, AAOD_{DUST} (except Karachi and Pokhara), AAOD_{BC} (except Lahore), and AAOD_{BrC} are all decreasing over these sites (Figs. 5–8). This is an indication of the increasing contribution of the scattering AOD to AOD. With regards to AAOD_{BrC} it has either no trend (similar to Kanpur) or a slightly decreasing trend over the observation at each site. The amount of dust that gets transported exhibits a gradient with decreasing concentrations with higher concentrations in the west and lower in the east across the IGP (Ramachandran et al., 2015, 2020a,b). AAOD_{BC} decreases while AAOD_{BrC} exhibits no trend over Gandhi College (Fig. 7i), suggesting that the contribution of BrC from biomass and biofuel burning, and fossil fuel emissions did not change over the region surrounding Gandhi College during the last decade. A previous study reported that aerosols over Pokhara are primarily influenced by urban/industrial and biomass burning emissions (Ramachandran and Rupakheti, 2020). Declining trends in both AAOD_{BC} and AAOD_{BrC} (Fig. 8i) over this site indicate a decrease in the amount of emissions of BC and BrC from the above sources in the recent years within Pokhara Valley and surrounding region (Sadavarte et al., 2019). In general, the rate of decline in AAOD_{BrC}

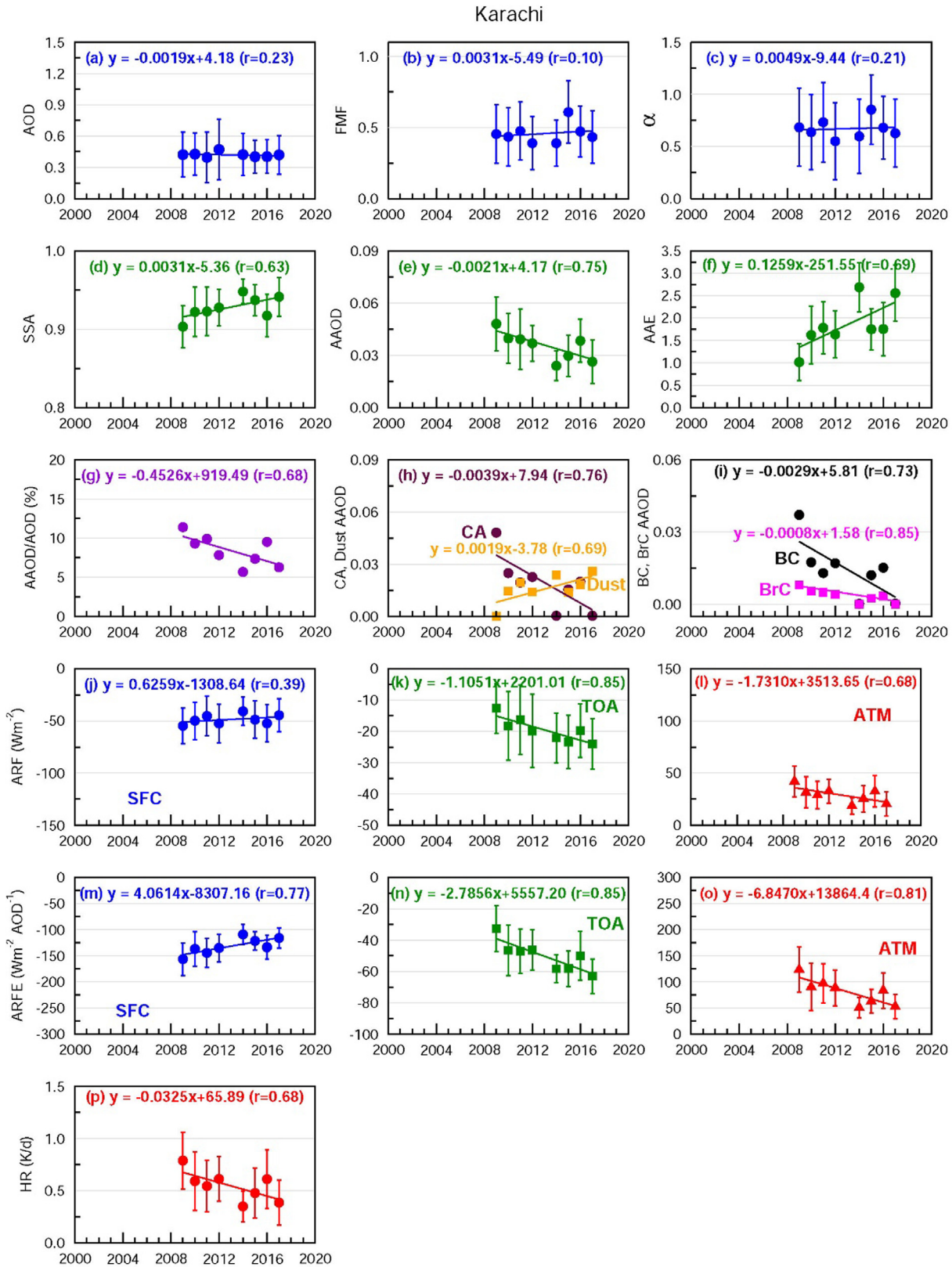


Fig. 5. Aerosol characteristics and radiative forcing over Karachi, Pakistan in the IGP during 2009–2017 based on the AERONET measurements. The aerosol parameters are presented in the same order as in Fig. 3.

is lower than that of the increase/decrease in AAOD_{BC} at each site during the measurement period. Therefore, the trends in SSA and these parameters indicate that the aerosols over South Asia are becoming less absorbing.

The ARF_{SFC} is increasing while the ARF_{TOA} and ARF_{ATM} are decreasing over all the sites (Figs. 5–8) except Lahore where ARF_{ATM} shows an increasing trend (Fig. 6l). The trends in ARFE follow the trends in ARF. The HR at all sites in South Asia (except

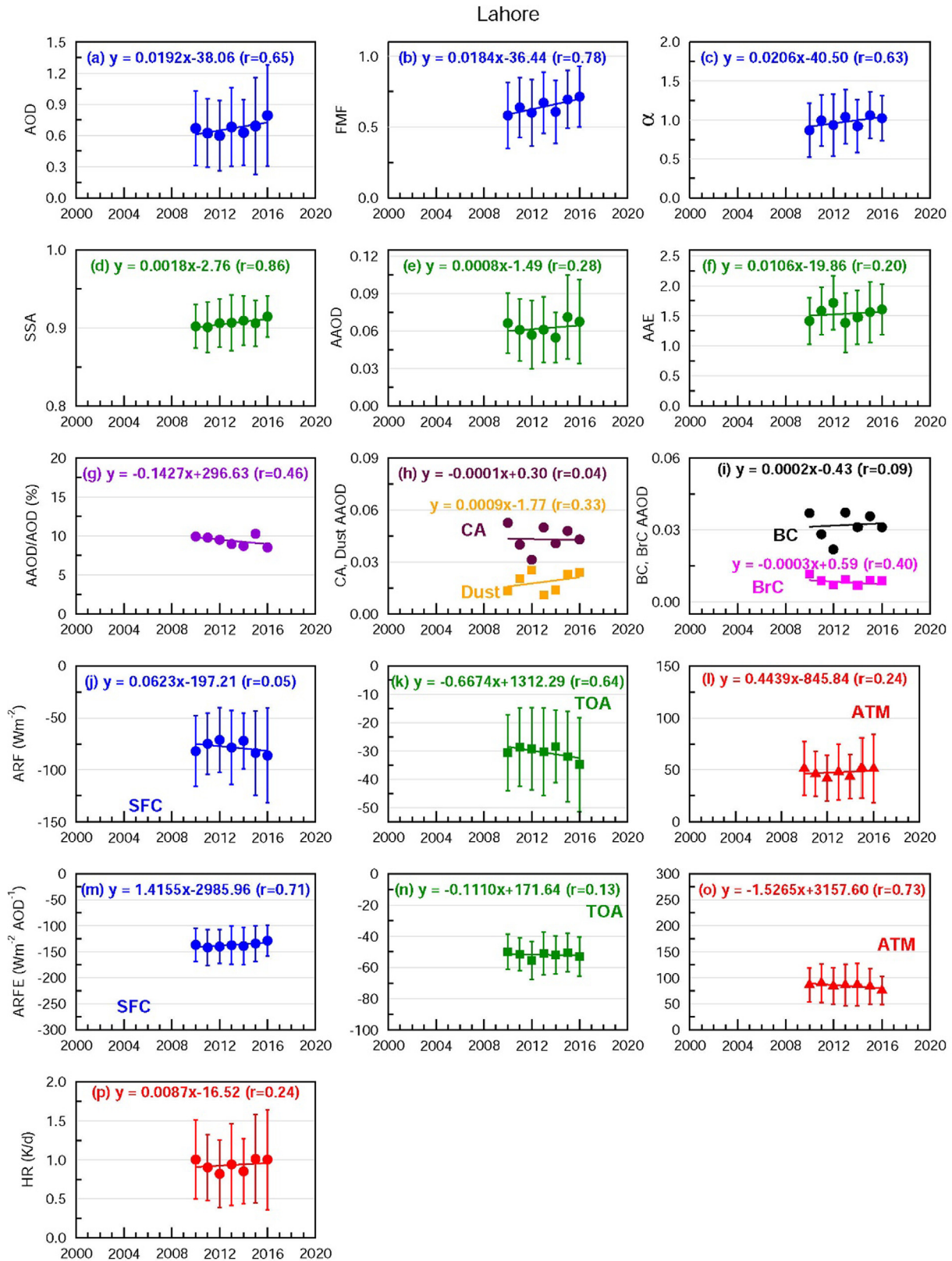


Fig. 6. Aerosol characteristics and radiative forcing over Lahore, Pakistan in the IGP during 2010–2016 based on the AERONET measurements. The aerosol parameters are presented in the same order as in Fig. 3.

Lahore, Fig. 6p) exhibits decreasing trends (Figs. 5p, 7p, 8p) consistent with the trend over Kanpur, however, the rates of decrease differ; for example, over Karachi HR decreased at a significantly

higher rate. The trends in absorbing aerosol characteristics (AAOD, AAOD_{CA}, AAOD_{Dust}, AAOD_{BC} and AAOD_{BrC}) and ARF (TOA) and ARFE (SFC, TOA and ATM) over Karachi (Fig. 5) are significant at 95%

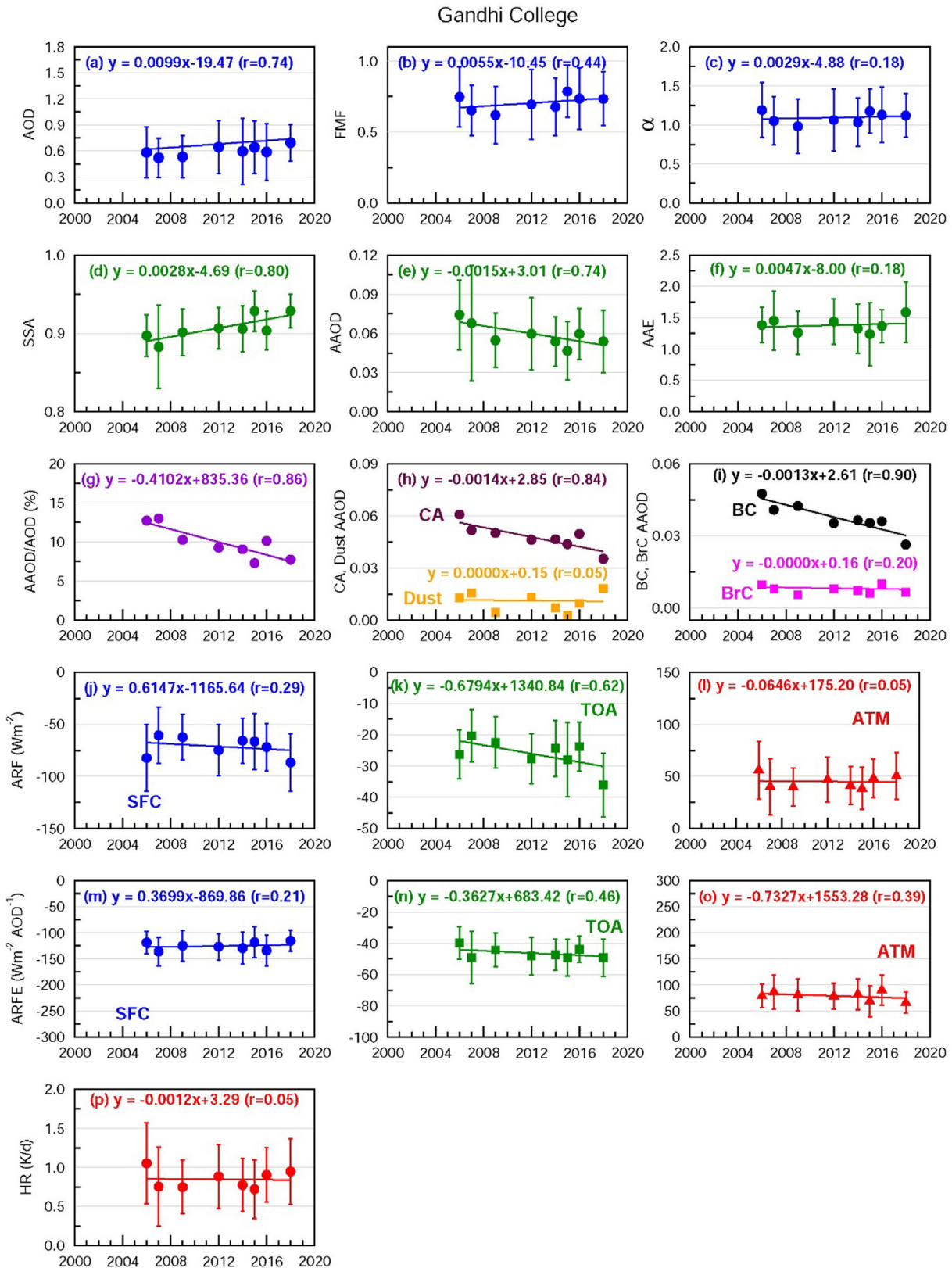


Fig. 7. Aerosol characteristics and radiative forcing over Gandhi College, India in the IGP during 2006–2018 based on the AERONET measurements. The aerosol parameters are presented in the same order as in Fig. 3.

confidence level with p-values ≤ 0.05 (Table 2). It should be noted that such low p-values (meaning high significance in trends) over Karachi are explicit in 8-year data as compared to Kanpur and Beijing both of which have data records twice as long.

The p-value for trend in AHR over Karachi is a little higher at 0.06 (Fig. 5p, Table 2). The HR over South Asian sites (Figs. 3p, 6p, 7p, 8p) except Karachi is still $>0.8 \text{ K d}^{-1}$ (Fig. 5p) whereas it has decreased to 0.5 K d^{-1} over Beijing (Fig. 4p).

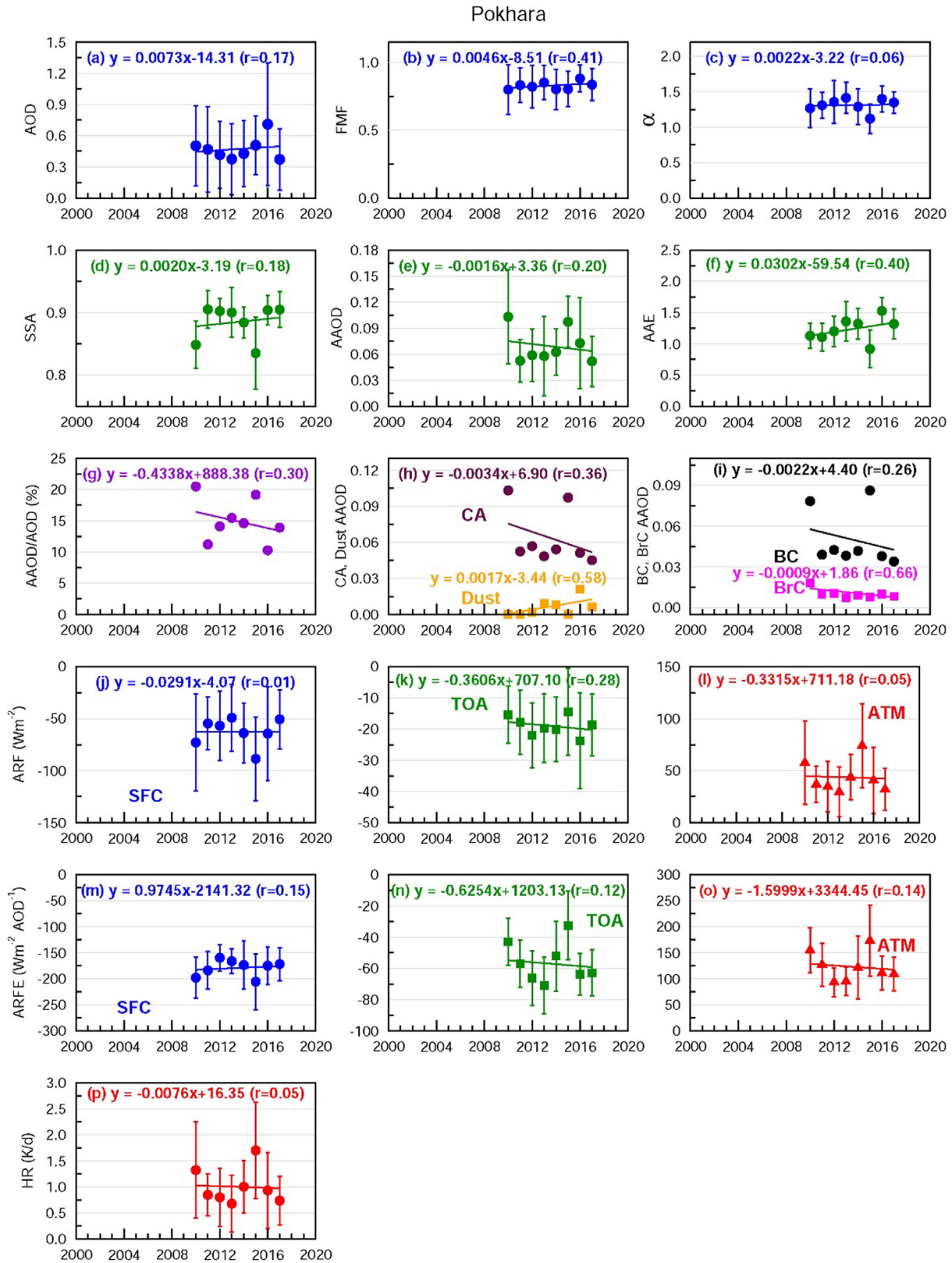


Fig. 8. Aerosol characteristics and radiative forcing over Pokhara, Nepal in the Himalayan foothills during 2010–2017 based on the AERONET measurements. The aerosol parameters are presented in the same order as in Fig. 3.

3.2.3.2. *NCP – Xianghe.* AOD shows a decreasing trend in Xianghe (Fig. 9a) similar to Beijing (Fig. 4a), however, FMF shows a slight positive trend whereas over Beijing FMF trend is negative (Figs. 4b, 9b). No trend in α and SSA is visible over Xianghe. In con-

trast SSA over Beijing shows a significantly strong increasing trend (Table 2). AAOD shows a slight decrease over Xianghe during the last 2-decades (Fig. 9e), while AAE shows an increasing trend (Fig. 9f), however, the trend in AAE is a factor of 2 less than Beijing

(Fig. 4f). Owing to a smaller decrease in AOD and no trend in AAOD as compared to Beijing AAOD/AOD ratio over Xianghe shows an increasing trend (Fig. 9g). AAOD_{CA} shows a decreasing trend

(Fig. 9h) similar to Beijing, however, the rate of decrease is 3-times higher over Beijing, whereas the increasing trend in AAOD_{Dust} is 1.5-times higher over Xianghe. Similar to the trend

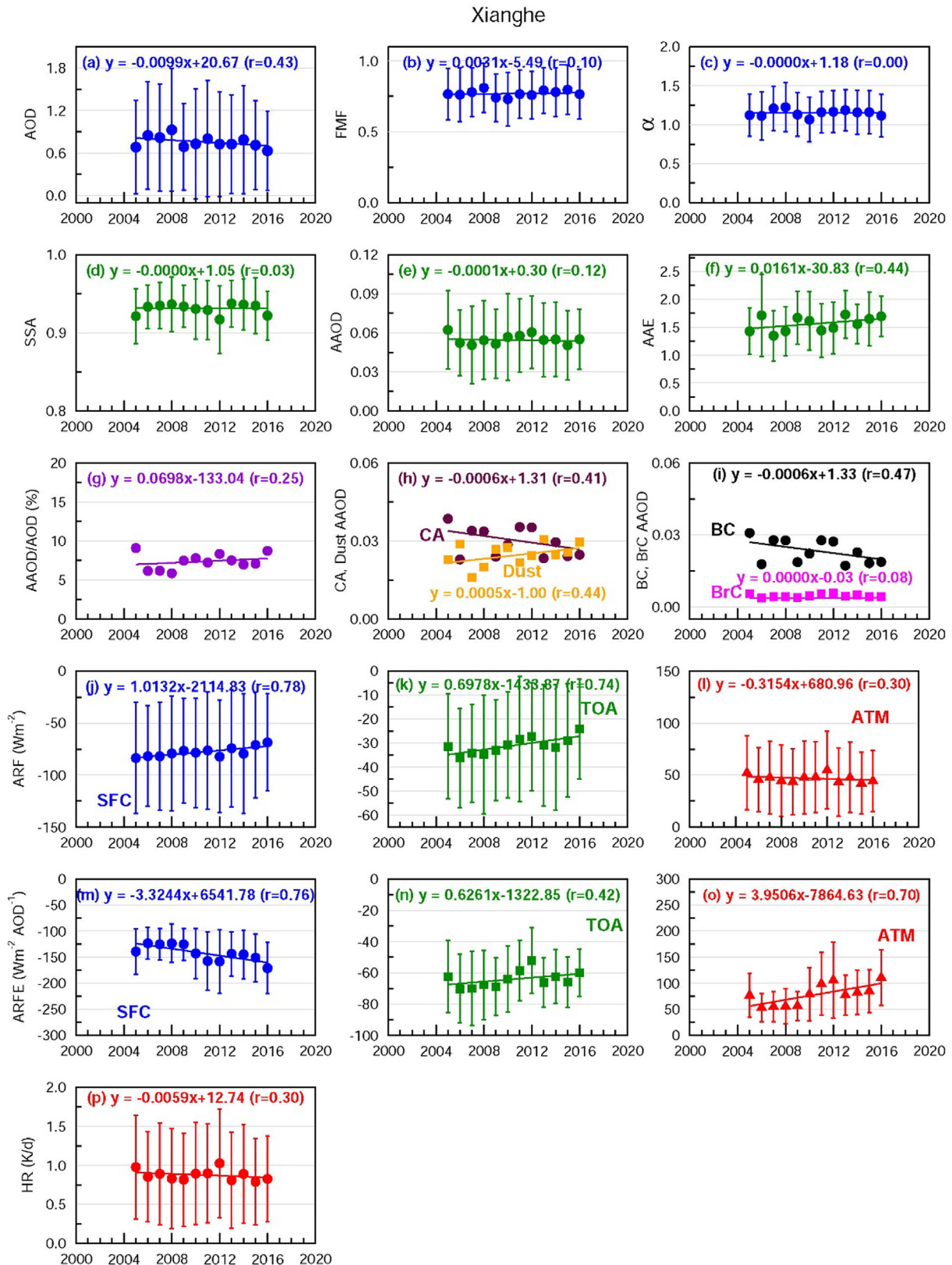


Fig. 9. Aerosol characteristics and radiative forcing over Xianghe, China in the NCP during 2005–2016 based on the AERONET measurements. The aerosol parameters are presented in the same order as in Fig. 3.

in $AAOD_{CA}$ the $AAOD_{BC}$ also shows a decreasing trend over Xianghe (Fig. 9i), and the rate of decrease is same as that of $AAOD_{CA}$ (indicating that the decreasing trend is largely controlled by BC) and 3-times lower compared to Beijing (Figs. 4 and 9). The increasing trends in ARF_{SFC} and ARF_{TOA} are significant at 95% CL (p -values < 0.05), while ARF_{ATM} exhibits a decreasing trend (Fig. 9l). $ARFE_{SFC}$ decreases over Xianghe similar to Beijing and is significant. $ARFE_{TOA}$ and $ARFE_{ATM}$ show increasing trends in contrast to Beijing (Figs. 4 and 9). They show increasing trends because ARF_{TOA} and ARF_{ATM} also increased while AOD decreased, however, not so significantly. The decrease in HR over Xianghe is only marginal during 2-decades, decreasing from 0.98 Kd^{-1} in 2005 to 0.83 Kd^{-1} in 2016, similar to marginal decrease in ARF_{ATM} (Fig. 9l, p). The HR over Xianghe is almost 2-times higher than Beijing now. The near similar values of SSA during 2005–2016 over Xianghe suggests that the chemical composition of aerosols has not changed significantly, while the columnar content (AOD) decreased similar to Beijing. It is clear from these results despite some specific difference in magnitude of aerosol properties both Beijing and Xianghe show largely similar aerosol characteristics indicating a regional scale change in columnar aerosol properties over NCP.

4. Implications

The sites in South Asia have generally regionally homogenous aerosol properties, except some site-specific properties in terms of their absolute and relative contributions due to their locations in/near specific prominent emission sources. The trends in aerosol column content are different between South Asia and East Asia, while the changes in composition (SSA) are of the same sign suggesting that aerosols are becoming more scattering in nature over both South Asia and East Asia (Figs. 2–9). The response of climate to aerosol loading, composition and radiative effects over Asia is highly uncertain (Samset et al., 2019). The model simulations of Asian monsoon's response to aerosol perturbation, and representation of precipitation over the Asian region are uncertain (Samset et al., 2019). The emerging divergence in aerosol loadings (and associated changes in aerosol composition) seen between East Asia and South Asia (Figs. 2–9) adds another dimension in the complex aerosol-climate interactions over Asia. It is clear from our analysis that accelerated reduction in aerosol emissions yield significant climate benefits in addition to significant improvement in air quality and reduction in adverse health impacts. The control in aerosol emissions certainly lead to a reduction in the column content of aerosols (AOD) and change in the composition (SSA) (Figs. 2–9). Thus, it is important to carefully decide what type(s) of aerosol species (e.g., BC vs. sulfate) need to be reduced at what proportion concurrently that can result in a significant decline in column content as well as atmospheric warming. This underlines the emergent need to reduce emissions of SO_2 concurrently with a larger reduction in emissions of BC, resulting in an increase in the contribution of scattering aerosols (i.e., higher SSA), which will in turn lead to climate cooling or reduction in atmospheric warming. Both the primary as well as secondary aerosols need to be reduced to account for the complex interactions between the different types of air pollutants. However, in the context of changing aerosol regime the emissions of primary aerosols are decreasing but the proportions of the secondary aerosols in ambient aerosols are increasing (Huang et al., 2014) which can influence the hygroscopicity of aerosols (Li et al., 2021). In addition, surface ozone, a strong atmospheric oxidant, is also increasing over China (Li et al., 2019). The surface ozone has increased due partly to the decrease in $\text{PM}_{2.5}$ which slowed down the aerosol sink of hydroperoxy radical and enhanced ozone production (Li et al., 2019). In case of South Asia, where $\text{PM}_{2.5}$ and ozone are expected to increase in the coming dec-

ades (Kumar et al., 2018), the secondary aerosols and ozone need to be taken into account carefully for mitigation of both air pollution and climate change.

The annual mean aerosol-induced atmospheric solar heating rate is consistently high and regionally coherent every year for almost two decades over both South Asia and East Asia. The ARFE values obtained from observations over South Asia including the Himalayas and Beijing in East Asia are at least 2–4 times higher than those obtained in previous studies over the study regions surrounding the Himalayas, for example over the Indian Ocean (Ramanathan et al., 2007a,b), Kanpur (IGP), Beijing (China), and Gosan (S. Korea) (Cho et al., 2017). Models grossly underestimate ARFE over this region (Cho et al., 2017). The heating rate (Figs. 3–9) is comparable to the heating rate obtained in spring 2008 for the plumes from Beijing (East Asia) (Ramana et al., 2010), and at least twice as high compared to the reported heating rate ($0.45\text{--}0.7 \text{ K day}^{-1}$) during spring 2006 over the Indian Ocean (Ramanathan et al., 2007a; Ramana et al., 2010) in South Asia. Though the heating rate is lower currently, it is still more than 0.5 K day^{-1} over Beijing and more than 0.8 K day^{-1} over all the locations in South Asia (except Karachi), and Xianghe in East Asia (Figs. 3–9), which has severe implications to climate (e.g., atmospheric warming and consequent impacts). The comparison covers only those results that are relevant and available over the study regions of South and East Asia, including the Indian Ocean, Indo-Gangetic Plain, the Himalayas and the North China Plain. It should be noted that in contrast to our comprehensive study with long-term records, the past studies mentioned above were based on limited set of measurements made during a particular season and/or over a particular location – over Maldives in the Indian Ocean during pre-monsoon using vertical profiles of scattering coefficients and absorption coefficients in altitude range between the surface and 3 km and the Monte Carlo Aerosol-Cloud Radiation (MACR) model (Ramanathan et al., 2007a), adopting the AERONET observations of AOD, the Ångström coefficient and SSA over Maldives in the MACR model during Oct 2004–Dec 2005 (Ramanathan et al., 2007b), ground-based and aerial measurements of BC and radiation during Aug–Sep 2008 over Beijing, Shanghai and Yellow Sea and the MACR model (Ramana et al., 2010), and ARF and ARFE were derived using the AERONET retrieved AOD, SSA and asymmetry parameter for Kathmandu and Kanpur in a column radiative model (Cho et al., 2017). In contrast, the results presented in our study, including ARFs and ARFEs are based on high-quality observations at multiple sites across a large region in Asia. The aerosol-induced atmospheric heating can alter regional atmospheric stability and vertical motions, affect large scale circulation and the hydrological cycle, affect sensitive ecosystems such as agro-ecosystems and cryosphere, and thus be accompanied with significant regional climate change and associated effects (Menon et al., 2002). The amplification of regional temperature increase, including elevation dependent warming, is attributed as a major cause for the Himalayan-Tibetan Plateau glacier melting (Krishnan et al., 2019). The rapid retreat of glaciers is expected to significantly affect negatively the regional hydrological cycle and the water supply in South and East Asia (Thompson et al., 2003; Barnett et al., 2005; Krishnan et al., 2019). The rapid and contrasting changes in aerosol forcing on inter-regional scale, as reported in our study, may result in climate effects that are noticeable over Asia and beyond, which include changes to mean and extreme temperature, precipitation, the onset and strength of the monsoon, availability of freshwater and changes to air quality (Samset et al., 2019). The observed evolution of aerosols (content and composition), and aerosol-induced heating rate changes to atmosphere, thus, calls for modelling efforts to better quantify the aerosol-climate interactions over Asia which has immense climate and health implications.

5. Summary and conclusions

Satellite observations and model simulations show that the geographical distributions of emissions of climate-forcing species have changed significantly in the last decade as a result of the economic and development activities and introduction of air quality management regulations in Asia. Satellite observations clearly show regional-scale changes in aerosol content (AOD) as well as composition (SSA) and absorption (Figs. 1 and 2) over Asia. This study reports for the first time, using high-quality ground-based aerosol data in several locations in South Asia and East Asia covering a large spatial domain that includes Pakistan, India, Nepal and China, the quantitative changes, and the trends in climate-relevant aerosol parameters (AOD, SSA, AAOD, ARF, ARFE, and HR) which are key to understand and simulate the complex aerosol-climate interactions and climate change.

The analysis of the aerosol loading (AOD) in the last 2-decades shows a positive (increasing) trend over Kanpur (and other locations in South Asia including over Pokhara, located at the foothills of the Himalayas often downwind of the Indo-Gangetic Plain), and a significant negative (decreasing) trend over Beijing and Xianghe (East Asia) clearly revealing a divergence in aerosol loading between these two global aerosol hotspots. The reduction in AOD over East Asia is a result of the decrease in aerosol emissions during the last decade due to implementation of strict regulations aimed at improving air quality in China.

The aerosol composition over these two regions is also changing in such a way that the aerosols are becoming less absorbing in nature. The positive (increasing) trend in SSA over both sub-regions in Asia is supported by the negative (decreasing) trends of AAOD, AAOD/AOD ratio, AAOD_{BC} and AAOD_{BrC}. AAOD due to carbonaceous aerosol (AAOD_{CA}) shows a decreasing trend at all the study locations, though the rates of decrease are different, it is about 3-times faster over Beijing in East Asia than Kanpur in South Asia. The AAOD due to dust (AAOD_{Dust}) is lower than AAOD_{CA} at all the locations. The AAOD_{Dust} shows differing spatial trends over Asia – it is decreasing over Kanpur, remaining almost constant over Gandhi College and increasing over Karachi, Lahore and Pokhara in the IGP, and over Xianghe and Beijing in NCP. Among the carbonaceous aerosols, BC contributes the most to the AAOD_{CA}, unequivocally confirming BC as the dominant light-absorbing aerosol (among BC, BrC and Dust) in South Asia (Ramachandran et al., 2020b) and East Asia (Cho et al., 2019). The AAOD_{BC} shows decreasing trends at all sites (except Lahore) considered in this study. The rate of decrease in AAOD_{BC} is 3-times higher over Beijing when compared to Kanpur. AAOD_{BrC} shows decreasing trend over all locations in South and East Asia (except Kanpur and Gandhi College where no clear trend was observed). Emissions of both SO₂ and BC have decreased over China, with the rate of decrease in BC emissions a half that of SO₂ during 2010–2018, which resulted in changing SSA values. The increase in SSA over Kanpur and other locations in South Asia can be attributed to the increasing SO₂ emissions in South Asia. The secondary organic aerosol compounds and surface ozone are also increasing which could have aided the increase in SSA values, that deserves attention in future studies.

The aerosol radiative forcing (ARF) at the Earth's surface (ARF_{SFC}) shows an increasing trend (i.e., becomes less negative or more sunlight is reaching the earth's surface) at all locations over South and East Asia. ARF at the top of the atmosphere (ARF_{TOA}) shows a decreasing trend at all other locations in South Asia, whereas over Beijing and Xianghe in East Asia it shows an increasing trend because only at these two locations AOD is decreasing. The ARF in the atmosphere (ARF_{ATM}) shows a decreasing trend at all locations over both South and East Asia (except Lahore where it has remained almost the same over the observation period).

The trends in the aerosol radiative forcing efficiency (ARFE) at the surface (ARFE_{SFC}) differ between the two regions, i.e., increasing over South Asia and decreasing over East Asia, which is indicative of the changes in ARFE differently. This occurs because AOD decreased significantly over East Asia during the last 2-decades whereas AOD increased over South Asia. In general, the ARFE_{TOA} decreased over both regions. ARFE_{ATM} decreased over South Asia while it remains almost the same or increased over East Asia. However, HR decreased during the last 2-decades over both South and East Asia. The rate of decrease is quite significant over Beijing, being 3-times faster than over Kanpur. The annual-mean HR even now is quite high over all sites in over both East Asia and South Asia (>0.5 K d⁻¹). A regionally coherent atmospheric heating of this magnitude has adverse implications to climate including temperature, hydrological cycle, melting of glaciers and snow fields with consequences not only over Asia on a regional scale but beyond.

Trends, derived on a variety of aerosol properties (content, composition, size and type) and radiative effects, for the first time over a large spatial domain that covers a wide range of varying environments (urban, rural, industrial to coastal) using high-quality data from the network with the same set of aerosol and radiation instruments, are very crucial to reduce the uncertainties in aerosol-induced atmospheric warming and climate change, and simulate better the aerosol-climate interaction in the present and future climate. The knowledge gained on absorbing aerosol type, contributions to aerosol absorption and their trends derived in this study over a large spatial domain can further be also used to validate the satellite retrievals and improve the retrieval algorithms.

Declaration of Competing Interest

The authors declare that they have no known competing financial interests or personal relationships that could have appeared to influence the work reported in this paper.

Acknowledgements

We thank the principal investigators for their efforts in establishing and maintaining the AERONET sites (<https://aeronet.gsfc.nasa.gov/>) the data of which are used in the study. This work was performed by SR as a Senior Fellow at IASS on a sabbatical from Physical Research Laboratory, India. Currently he is also an Affiliate Scholar of IASS. We are grateful to the German Federal Ministry for Education and Research (BMBF) and the Brandenburg State Ministry for Science, Research and Culture (MWFK) for funding the IASS. The MODIS Terra, and OMI OMAERUV v003 (level-2) data products were downloaded (Figs. 1 and 2) from <https://giovanni.gsfc.nasa.gov/giovanni/>, and https://disc.gsfc.nasa.gov/datasets/OMAERO_003/summary, respectively. We also acknowledge the MODIS and OMI mission scientists and associated NASA personnel for the production of the data used in Figs. 1 and 2.

References

- Adesina, A.J., Kumar, K.R., Sivakumar, V., Griffith, D., 2014. Direct radiative forcing of urban aerosols over Pretoria (25.75°S, 28.28°E) using AERONET Sunphotometer data: First scientific results and environmental impact. *J. Environ. Sci.* 26, 2459–2474.
- Andrews, E., Ogren, J.A., Kinne, S., Samsel, B., 2017. Comparison of AOD, AAOD and column single scattering albedo from AERONET retrievals and in situ profiling measurements. *Atmos. Chem. Phys.* 17, 6041–6072. <https://doi.org/10.5194/acp-17-6041-2017>.
- Arimoto, R., Kim, Y.J., Kim, Y.P., Quinn, P.K., Bates, T.S., Anderson, T.L., Gong, S., Uno, I., Chin, M., Huebert, B.J., Clarke, A.D., Shinozuka, Y., Weber, R.J., Anderson, J.R., Guazzotti, S.A., Sullivan, R.C., Sodeman, D.A., Prather, K.A., Sokolik, I.N., 2006.

- Characterization of Asian dust during ACE-Asia. *Global Planet. Change* 52 (1–4), 23–56.
- Barnett, T.P., Adam, J.C., Lettenmaier, D.P., 2005. Potential impact of a warming climate on water availability in snow-dominated regions. *Nature* 438, 303–309.
- Cao, Y., Shao, L., Jones, T., Oliveira, M.L.S., Ge, S., Feng, X., Silva, L.F.O., BêruBê, K., 2021. Multiple relationships between aerosol and COVID19: A framework for global studies. *Gondwana Res.* 93, 243–251.
- Che, H., Xia, X., Zhao, H., Dubovik, O., Holben, B.N., Goloub, P., Cuevas-Agulló, E., Estelles, V., Wang, Y., Zhu, J., Qi, B., Gong, W., Yang, H., Zhang, R., Yang, L., Chen, J., Wang, H., Zheng, Y., Gui, K., Zhang, X., Zhang, X., 2019. Spatial distribution of aerosol microphysical and optical properties and direct radiative effect from the China Aerosol Remote Sensing Network. *Estelles, V., Wang, Y., Zhu, J., Qi, B., Gong, W., Yang, H., Zhang, R., Yang, L., Chen, J., Wang, H., Zheng, Y., Gui, K., Zhang, X., Zhang, X., 2019. Atmos. Chem. Phys.*, 19, 11843–11864 (2019).
- Cho, C., Kim, S.-W., Lee, M., Lim, S., Fang, W., Gustafsson, O., Andersson, A., Park, R.J., Sheridan, P.J., 2019. Observation-based estimates of the mass absorption cross-section of black carbon and brown carbon and their contribution to aerosol light absorption in East Asia. *Atmospheric Environment* 212, 65–74. <https://doi.org/10.1016/j.atmosenv.2019.05.024>.
- Cho, C., Kim, S.-W., Rupakheti, M., Park, J.-S., Panday, A., Yoon, S.-C., Kim, J.-H., Kim, H., Jeon, H., Sung, M., Kim, B.M., Hong, S.K., Park, R.J., Rupakheti, D., Mahata, K.S., Praveen, P.S., Lawrence, M.G., Holben, B., 2017. Wintertime aerosol optical and radiative properties in the Kathmandu Valley during the SusKat-ABC field campaign. *Atmos. Chem. Phys.* 17 (20), 12617–12632.
- Choi, J.-O., Chung, C.E., 2014. Sensitivity of aerosol direct radiative forcing to aerosol vertical profile. *Tellus B: Chemical and Physical Meteorology* 66 (1). <https://doi.org/10.3402/tellusb.v66.24376>.
- Chung, C.E., Ramanathan, V., Decremer, D., 2012. Observationally constrained estimates of carbonaceous aerosol radiative forcing. *Proc. Nat. Acad. Sci.* 109 (29), 11624–11629.
- Dubovik, O., 2006. Application of spheroid models to account for aerosol particle nonsphericity in remote sensing of desert dust. *Journal of Geophysical Research* 111 (D11208), 1–34. <https://doi.org/10.1029/2005JD006619>.
- Dubovik, O., Smirnov, A., Holben, B.N., King, M.D., Kaufman, Y.J., Eck, T.F., Schuster, I., 2000. Accuracy assessments of aerosol optical properties retrieved from Aerosol Robotic Network (AERONET) Sun and Sky radiance measurements. *J. Geophys. Res.* 105, 9791–9806.
- Dubuisson, P., Buriez, J.C., Fouquart, Y., 1996. High spectral resolution solar radiative transfer in absorbing and scattering media: Application to the satellite simulation. *J. Quant. Spec. Rad. Tran.* 55, 103–126.
- García, O.E., Díaz, A.M., Expósito, F.J., Díaz, J.P., Dubovik, O., Dubuisson, P., Roger, J.-C., Eck, T.F., Sinyuk, A., Derimian, Y., Dutton, E.G., Schafer, J.S., Holben, B.N., García, C.A., 2008. Validation of AERONET estimates of atmospheric solar fluxes and aerosol radiative forcing by ground-based broadband measurements. *J. Geophys. Res.* 113 (D21). <https://doi.org/10.1029/2008JD010211>.
- García, O.E., Díaz, J.P., Expósito, F.J., Díaz, A.M., Dubovik, O., Derimian, Y., Dubuisson, P., Roger, J.-C., 2012. Shortwave radiative forcing and efficiency of key aerosol types using AERONET data. *Atmos. Chem. Phys.* 12 (11), 5129–5145.
- Giles, D.M., Sinyuk, A., Sorokin, M.G., Schafer, J.S., Smirnov, A., Slutsker, I., Eck, T.F., Holben, B.N., Lewis, J.R., Campbell, J.R., Welton, E.J., Korkin, S.V., Lyapustin, A.I., 2019. Advancements in the Aerosol Robotic Network (AERONET) version 3 database – automated near-real-time quality control algorithm with improved cloud screening for Sun photometer aerosol optical depth measurements. *Atmos. Meas. Tech.* 12, 169–209.
- Hess, M., Koepke, P., Schult, I., 1998. Optical properties of aerosols and clouds: The software package OPAC. *Bull. American Meteorol. Soc.* 79 (5), 831–844.
- Hoegh-Guldberg, O., D. Jacob, M. Taylor, M. Bindi, S. Brown, I. Camilloni, A. Diedhiou, R. Djalante, K.L. Ebi, F. Engelbrecht, J. Guiot, Y. Hijikata, S. Mehrotra, A. Payne, S.I. Seneviratne, A. Thomas, R. Warren, and G. Zhou, 2018: Impacts of 1.5°C Global Warming on Natural and Human Systems. In: *Global Warming of 1.5°C: An IPCC Special Report on the impacts of global warming of 1.5°C above pre-industrial levels and related global greenhouse gas emission pathways, in the context of strengthening the global response to the threat of climate change, sustainable development, and efforts to eradicate poverty* [Masson-Delmotte, V., P. Zhai, H.-O. Pörtner, D. Roberts, J. Skea, P.R. Shukla, A. Pirani, W. Moufouma-Okia, C. Péan, R. Pidcock, S. Connors, J.B.R. Matthews, Y. Chen, X. Zhou, M.I. Gomis, E. Lonnoy, T. Maycock, M. Tignor, and T. Waterfield (eds.)], IPCC, 175–312.
- Holben, B.N., Tanré, D., Smirnov, A., Eck, T.F., Slutsker, I., Abuhassan, N., Newcomb, W.W., Schafer, J.S., Chatenet, B., Lavenu, F., Kaufman, Y.J., Castle, J.V., Setzer, A., Markham, B., Clark, D., Frouin, R., Halthore, R., Karneli, A., O'Neill, N.T., Pietras, C., Pinker, R.T., Voss, K., Zibordi, G., 2001. An emerging ground-based aerosol climatology: Aerosol optical depth from AERONET. *J. Geophys. Res.* 106 (D11), 12067–12097.
- Huang, R.-J., Zhang, Y., Bozzetti, C., Ho, K.-F., Cao, J.-J., Han, Y., Daellenbach, K.R., Slowik, J.G., Platt, S.M., Canonaco, F., Zotter, P., Wolf, R., Pieber, S.M., Bruns, E.A., Crippa, M., Ciarelli, G., Piazzalunga, A., Schwikowski, M., Abbaszade, G., Schnelle-Kreis, J., Zimmermann, R., An, Z., Szidat, S., Baltensperger, U., Haddad, I.E., Prévôt, A.S.H., 2014. High secondary aerosol contribution to particulate pollution during haze events in China. *Nature* 514 (7521), 218–222.
- IEA, 2016. *World Energy Outlook 2016*. IEA, Paris. <https://www.iea.org/reports/world-energy-outlook-2016>.
- IPCC, 2013. *Summary for Policymakers in Climate Change 2013: The Physical Science Basis. Contribution of Working Group I to the Fifth Assessment Report of the Intergovernmental Panel on Climate Change*. Stocker, T.F., Qin, D., Plattner, G.-K., Tignor, M., Allen, S.K., Boschung, J., Nauels, A., Xia, Y., Bex, V., Midgley, P.M., (Eds.), Cambridge Univ. Press, Cambridge, UK. And NY, USA, 1–33 (2013).
- Jethva, H., Torres, O., Ahn, C., 2014. Global assessment of OMI aerosol single-scattering albedo using ground-based AERONET inversion. *Journal of Geophysical Research Atmospheres* 119, 9020–9040. <https://doi.org/10.1002/2014JD021672>.
- Jethva, H., Chand, D., Torres, O., Gupta, P., Lyapustin, A., Patadia, F., 2018. Agricultural burning and air quality over northern India: A synergistic analysis using NASA's A-train satellite data and ground measurements. *Aerosol Air Qual. Res.* 18 (7), 1756–1773.
- Jethva, H., Torres, O., Field D., R., Lyapustin, A., Gautam, R., Kayetha, V., 2019. Connecting crop productivity, residue fires, and air quality over northern India. *Scientific Reports* 9. <https://doi.org/10.1038/s41598-019-52799-x>.
- Kedia, S., Ramachandran, S., Holben, B.N., Tripathi, S.N., 2014. Quantification of aerosol type, and sources of aerosols over the Indo-Gangetic Plain. *Atmos. Environ.* 98, 607–619.
- Khan, R., Kumar, K.R., Zhao, T., 2019. The climatology of aerosol optical thickness and radiative effects in Southeast Asia from 18-years of ground-based observations. *Environ. Poll.* 254, 113025. <https://doi.org/10.1016/j.envpol.2019.113025>.
- Kirillova, E.N., Marinoni, A., Bonasoni, P., Vuillermoz, E., Facchini, M.C., Fuzzi, S., Decesari, S., 2016. Light absorption properties of brown carbon in the high Himalayas. *J. Geophys. Res.* 121 (16), 9621–9639.
- Krishnan, R., Shrestha, A.B., Ren, G., Rajbhandari, R., Saeed, S., Sanjay, J., Syed, M.A., Vellore, R., Xu, Y., You, Q., Ren, Y., 2019. Unravelling climate change in the Hindu Kush Himalaya: Rapid warming in the mountains and increasing extremes in The Hindu Kush Himalaya Assessment. In: P. Wester, A. Mishra, A. Mukherji and A.B. Shrestha (Eds.), 57–97 pp.
- Kumar, R., Barth, M.C., Pfister, G.G., Delle Monache, L., Lamarque, J.F., Archer-Nicholls, S., Tilmes, S., Ghude, S.D., Wiedinmyer, C., Naja, M., Walters, S., 2018. How will air quality change in South Asia by 2050? *J. Geophys. Res.* 123 (3), 1840–1864.
- Levy, R.C., Mattoo, S., Munchak, L.A., Remer, L.A., Sayer, A.M., Patadia, F., Hsu, N.C., 2013. The collection 6 MODIS aerosol products over land and ocean. *Atmos. Meas. Tech.* 6 (11), 2989–3034.
- Li, C., McLinden, C., Fioletov, V., Krotkov, N., Carn, S., Joiner, J., Streets, D., He, H., Ren, X., Li, Z., Dickerson, R.R., 2017. India is overtaking China as the world's largest emitter of anthropogenic sulfur dioxide. *Sci. Rep.* 7, 14304.
- Li, K.e., Jacob, D.J., Liao, H., Shen, L.u., Zhang, Q., Bates, K.H., 2019. Anthropogenic drivers of 2013–2017 trends in summer surface ozone in China. *Proc. Natl. Acad. Sci.* 116 (2), 422–427.
- Li, W., Shao, L., Wang, W., Li, H., Wang, X., Li, Y., Li, W., Jones, T., Zhang, D., 2020. Air quality improvement in response to intensified control strategies in Beijing during 2013–2019. *Sci. Total Environ.* 744 (140776), 2020.
- Li, W., Liu, L., Zhang, J., Xu, L., Wang, Y., Sun, Y., Shi, Z., 2021. Microscopic evidence for phase separation of organic species and inorganic salts in fine ambient aerosol particles. *Environ. Sci. Tech.* 55 (4), 2234–2242.
- Lim, S., Lee, M., Kim, S.-W., Laj, P., 2018. Sulfate alters aerosol absorption properties in East Asian outflow. *Scientific Reports* 8. <https://doi.org/10.1038/s41598-018-23021-1>.
- Mallet, M., Dubovik, O., Nabat, P., Dulac, F., Kahn, R., Sciare, J., Paronis, D., Léon, J.F., 2013. Absorption properties of Mediterranean aerosols obtained from multi-year ground-based remote sensing observations. *Atmos. Chem. Phys.* 13 (18), 9195–9210.
- Meng, J., Yang, H., Yi, K., Liu, J., Guan, D., Liu, Z., Mi, Z., Coffman, D.M., Wang, X., Zhong, Q., Huang, T., Meng, W., Tao, S., 2019. The slowdown in global air-pollutant emission growth and driving factors. *One Earth* 1 (1), 138–148.
- Menon, S., Hansen, J., Nazarenko, L., Luo, Y., 2002. Climate effects of black carbon aerosols in China and India. *Science* 297, 2250–2253.
- Mishchenko, M.I., Travis, L.D., Kahn, R.A., West, R.A., 1997. Modeling phase functions for dustlike tropospheric aerosols using a shape mixture of randomly oriented polydisperse spheroids. *J. Geophys. Res.* 102 (D14), 16831–16847.
- Myhre, G., 2013. Radiative forcing of the direct effect from AeroCom Phase II simulations. *Atmospheric Chemistry and Physics* 13, 1853–1877.
- Myhre, G. et al., 2017. Multi-model simulations of aerosol and ozone radiative forcing due to anthropogenic emission changes during the period 1990–2015. *Atmos. Chem. Phys.* 17, 2709–2720.
- O'Neill, N.T., Eck, T.F., Smirnov, A., Holben, B.N., Thulasiraman, S., 2003. Spectral discrimination of coarse and fine mode optical depth. *J. Geophys. Res.* 108. <https://doi.org/10.1029/2002JD002975>.
- Ozone Monitoring Instrument (OMI) Data User's Guide, NASA, 2012. 1–66 pp.
- Ramachandran, S., Kedia, S., Srivastava, R., 2012. Aerosol optical depth trends over different regions of India. *Atmos. Environ.* 49, 338–347.
- Ramachandran, S., Kedia, S., Sheel, V., 2015. Spatiotemporal characteristics of aerosols in India: Observations and model simulations. *Atmos. Environ.* 116, 225–244.
- Ramachandran, S., Rupakheti, M., 2020. Inter-annual and seasonal variations in columnar aerosol characteristics and radiative effects over the Pokhara Valley in the Himalayan foothills – Composition, radiative forcing, and atmospheric heating. *Environ. Poll.* 264, 114799. <https://doi.org/10.1016/j.envpol.2020.114799>.
- Ramachandran, S., Rupakheti, M., Lawrence, M.G., 2020a. Aerosol-induced atmospheric heating rate decreases over South and East Asia as a result of changing content and composition. *Sci. Rep.* 10, 20091.

- Ramachandran, S., Rupakheti, M., Lawrence, M.G., 2020b. Black carbon dominates the aerosol absorption over the Indo-Gangetic Plain and the Himalayan foothills. *Environ. Int.* 142, 105814. <https://doi.org/10.1016/j.envint.2020.105814>.
- Ramana, M.V., Ramanathan, V., Feng, Y., Yoon, S.-C., Kim, S.-W., Carmichael, G.R., Schauer, J.J., 2010. Warming influenced by the ratio of black carbon to sulphate and the black-carbon source. *Nature Geosci.* 3 (8), 542–545.
- Ramanathan, V., Ramana, M.V., Roberts, G., Kim, D., Corrigan, C., Chung, C., Winker, D., 2007a. Warming trends in Asia amplified by brown cloud absorption. *Nature* 448, 575–579.
- Ramanathan, V., Li, F., Ramana, M.V., Praveen, P.S., Kim, D., Corrigan, C.E., Nguyen, H., Stone, E.A., Schauer, J.J., Carmichael, G.R., Adhikary, B., Yoon, S.C., 2007b. Atmospheric brown clouds: Hemispherical and regional variations in long-range transport, absorption, and radiative forcing. *J. Geophys. Res.* 112 (D22). <https://doi.org/10.1029/2006JD008124>.
- Rupakheti, D., Kang, S., Rupakheti, M., Cong, Z., Panday, A.K., Holben, B.N., 2019. Identification of absorbing aerosol types at a site in the northern edge of Indo-Gangetic Plain and a polluted valley in the foothills of the central Himalaya. *Atmos. Res.* 223, 15–23.
- Russell, P.B., Bergstrom, R.W., Shinzuka, Y., Clarke, A.D., DeCarlo, P.F., Jimenez, J.L., Livingston, J.M., Redemann, J., Dubovik, O., Strawa, A., 2010. Absorption Angstrom Exponent in AERONET and related data as an indicator of aerosol composition. *Atmos. Chem. Phys.* 10 (3), 1155–1169.
- Sadavarte, P., Venkataraman, C., 2014. Trends in multi-pollutant emissions from a technology-linked inventory for India: I. Industry and transport sectors. *Atmos. Environ.* 99, 353–364.
- Sadavarte, P., Rupakheti, M., Bhawe, P., Shakya, K., Lawrence, M., 2019. Nepal Emission Inventory –Part I: Technologies and combustion sources (NEEMI-Tech) for 2001–2016. *Atmos. Chem. Phys.* 19 (20), 12953–12973.
- Samset, B.H., Lund, M.T., Bollasina, M., Myhre, G., Wilcox, L., 2019. Emerging Asian aerosol patterns. *Nature Geosci.* 12 (8), 582–584.
- Sayer, A.M., Munchak, L.A., Hsu, N.C., Levy, R.C., Bettenhausen, C., Jeong, M.-J., 2014. MODIS Collection 6 aerosol products: Comparison between Aqua's e-Deep Blue, Dark Target, and “merged” data sets, and usage recommendations. *J. Geophys. Res.* 119 (24), 13,965–13,989.
- Sayer, A.M., Knobelspiess, K.D., 2019. How should we aggregate data? Methods accounting for the numerical distributions, with an assessment of aerosol optical depth. *Atmos. Chem. Phys.* 19, 15023–15048.
- Schafer, J.S., Eck, T.F., Holben, B.N., Thornhill, K.L., Anderson, B.E., Sinyuk, A., Giles, D. M., Winstead, E.L., Ziemba, L.D., Beyersdorf, A.J., Kenny, P.R., Smirnov, A., Slutsker, I., 2014. Intercomparison of aerosol single-scattering albedo derived from AERONET surface radiometers and LARGO in situ aircraft profiles during the 2011 DRAGON-MD and DISCOVER-AQ experiments. *J. Geophys. Res.* 119 (12), 7439–7452. <https://doi.org/10.1002/2013JD021166>.
- Sogacheva, L., Rodriguez, E., Kolmonen, P., Virtanen, T.H., Saponaro, G., de Leeuw, G., Georgoulias, A.K., Alexandri, G., Kourtidis, K., van der A. J., 2018. Spatial and seasonal variations of aerosols over China from two decades of multi-satellite observations – Part 2: AOD time series for 1995–2017 combined from ATSR ADV and MODIS C6.1 and AOD tendency estimations. *Atmos. Chem. Phys.* 18, 16631–16652.
- Shindell, D., 2013. Radiative forcing in the ACCMIP historical and future climate simulations. *Atmospheric Chemistry and Physics* 13, 2939–2974. <https://doi.org/10.5194/acp-13-2939-2013>.
- Thompson, L.G., Thompson, E.M., Davis, M.E., Lin, P.-N., Henderson, K., Mashiotta, T. A., 2003. Tropical glacier and ice core evidence of climate changes on annual to millennial time scales. *Clim. Change* 59, 137–155.
- Torres, O., Bhartia, P.K., Jethva, H., Ahn, C., 2018. Impact of the ozone monitoring instrument row anomaly on the long-term record of aerosol products. *Atmos. Meas. Tech.* 11 (5), 2701–2715.
- Venkataraman, C., Brauer, M., Tibrewal, K., Sadavarte, P., Ma, Q., Cohen, A., Chaliyakunnel, C., Frostad, J., Klimont, Z., Martin, R.V., Millet, D.B., Philip, S., Walker, K., Wang, S., 2018. Source influence on emission pathways and ambient PM_{2.5} pollution over India (2015–2050). *Atmos. Chem. Phys.* 18, 8017–8039.
- Zhang, D., Zang, J., Shi, G., Iwasaka, Y., Matsuki, A., Trochne, D., 2003. Mixing states of individual Asian particles at a coastal site of Qingdao, China. *Atmos. Environ.* 37, 3895–3901.
- Zheng, B., Tong, D., Li, M., Liu, F., Hong, C., Geng, G., Li, H., Li, X., Peng, L., Qi, J., Yan, L., Zhang, Y., Zhao, H., Zheng, Y., He, K., Zhang, Q., 2018. Trends in China's anthropogenic emissions since 2010 as the consequence of clean air actions. *Atmos. Chem. Phys.* 18 (19), 14095–14111.